Report SAM-TR-79-4

② LEVEL II

RESEARCH ON THE OCULAR EFFECTS OF LASER RADIATION

Joseph A. Zuclich, Ph.D.
Gary A. Griess, Ph.D.
Joseph M. Harrison, Ph.D.
James C. Brakefield, M.S.E.E.
Life Sciences Division
Technology Incorporated
511 West Rhapsody Drive
San Antonio, Texas 78216

D D C
RECEIVED
MAY 1 1979
B

March 1979

Interim Report for Period 1 April 1977 — 31 March 1978

Approved for public release; distribution unlimited.
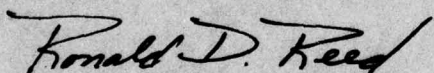
79 04 26 437

NOTICES

This interim report was submitted by Technology Incorporated, 511 West Rhapsody Drive, San Antonio, Texas 78216, under contract F33615-77-C-0615, job order 7757-02-58, with the USAF School of Aerospace Medicine, Aerospace Medical Division, AFSC, Brooks Air Force Base, Texas. First Lieutenant Ronald D. Reed (SAM/RZL) was the Laboratory Project Scientist-in-Charge.

When U.S. Government drawings, specifications, or other data are used for any purpose other than a definitely related Government procurement oper- ation, the Government thereby incurs no responsibility nor any obligation whatsoever; and the fact that the Government may have formulated, furnished, or in any way supplied the said drawings, specifications, or other data is not be regarded by implication or otherwise, as in any manner licensing the holder or any other person or corporation, or conveying any rights or per- mission to manufacture, use, or sell any patented invention that may in any way be related thereto.
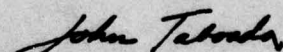
The animals involved in this study were procured, maintained, and used in accordance with the Animal Welfare Act of 1970 and the "Guide for the Care and Use of Laboratory Animals" prepared by the Institute of Laboratory Animal Resources - National Research Council.

This report has been reviewed by the Information Office (OI) and is releasable to the National Technical Information Service (NTIS). At NTIS, it will be available to the general public, including foreign nations.
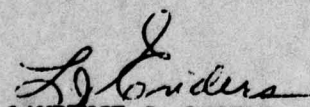
This technical report has been reviewed and is approved for publication.

RONALD D. REED, First Lieutenant, USAF
Project Scientist

JOHN TABOADA, Ph.D.
Supervisor

LAWRENCE J. ENDERS
Colonel, USAF, MC
Commander

REPORT DOCUMENTATION PAGE		READ INSTRUCTIONS BEFORE COMPLETING FORM
1. REPORT NUMBER SAM-TR-79-4	2. GOVT ACCESSION NO.	3. RECIPIENT'S CATALOG NUMBER
4. TITLE (and Subtitle) RESEARCH ON THE OCULAR EFFECTS OF LASER RADIATION		5. TYPE OF REPORT & PERIOD COVERED Interim rept. 1 April 77-31 March 78
		6. PERFORMING ORG. REPORT NUMBER
7. AUTHOR(s) Joseph A. Zuclich, James C. Brakefield, Gary A. Griess, Joseph M. Harrison		8. CONTRACT OR GRANT NUMBER(s) F33615-77-C-0615
9. PERFORMING ORGANIZATION NAME AND ADDRESS Life Sciences Division Technology Incorporated 511 West Rhapsody Drive, San Antonio, TX 78216		10. PROGRAM ELEMENT, PROJECT, TASK AREA & WORK UNIT NUMBERS 62202F 7757-02-58
11. CONTROLLING OFFICE NAME AND ADDRESS USAF School of Aerospace Medicine (RZL) Aerospace Medical Division (AFSC) Brooks Air Force Base, Texas 78235		12. REPORT DATE March 79
		13. NUMBER OF PAGES 74
14. MONITORING AGENCY NAME & ADDRESS(If different from Controlling Office)		15. SECURITY CLASS. (of this report) Unclassified
		15a. DECLASSIFICATION/DOWNGRADING SCHEDULE

16. DISTRIBUTION STATEMENT (of this Report)

Approved for public release; distribution unlimited.

17. DISTRIBUTION STATEMENT (of the abstract entered in Block 20, if different from Report)

DDC RECEIVED MAY 1 1979 B

18. SUPPLEMENTARY NOTES

19. KEY WORDS (Continue on reverse side if necessary and identify by block number)

Laser	Retina
Ocular Effects	Laser safety standards
Ultraviolet	Visual evoked response
Repetitive pulse	Visual function
Cornea	Visual stimulator

20. ABSTRACT (Continue on reverse side if necessary and identify by block number)

This report summarizes the accomplishments of the Life Sciences Division of Technology Incorporated during the first year (1 April 1977 through 31 March 1978) of Contract F33615-77-C-0615. The program has evolved into three independent projects studying ocular effects of ultraviolet laser radiation (discussed in Part I of this report), multiple-pulse effects (Part II), and pattern visual evoked response of laser-induced visual dysfunction (Part III).

DD FORM 1473 1 JAN 73   EDITION OF 1 NOV 65 IS OBSOLETE

SUMMARY

This report summarizes the accomplishments of the Life Sciences Division of Technology Incorporated during the first year (1 April 1977 through 31 March 1978) of Contract F33615-77-C-0615. The program has evolved into three independent projects studying ocular effects of ultraviolet laser radiation (discussed in Part I of this report), multiple-pulse effects (Part II), and pattern visual evoked response of laser-induced visual dysfunction (Part III).

Part I reports the observation of retinal damage from a helium-cadmium laser which was shown to exhibit self-mode-locking. The retinal threshold is nearly two orders of magnitude less than the corneal threshold for identical exposure parameters and represents an unanticipated ocular hazard from UV laser radiation.

Also discussed in Part I is a project designed to provide a quantitative evaluation of the cumulative nature of UV-induced corneal damage. The results presented indicate that there is only minimal recovery from the effects of subthreshold UV exposures in the 24-hour period following exposure. Indeed, recovery may not be complete until approximately 72 hours following the exposure.

Each of the projects mentioned above impacts upon existing safety standards for ocular exposure to near-UV laser radiation, so that Part I concludes with an examination of the existing standards and presents recommended changes.

The determination of multiple-pulse retinal thresholds in Macaca fascicularis monkeys is reported in Part II. This work found no more than a factor of two difference between the single-pulse threshold for 10-μsec, 514.5-nm argon laser pulses and multiple-pulse thresholds for trains of 10-μsec pulses at several repetition rates. This is in contrast to a previous report of much larger decrements in multiple-pulse relative to single-pulse thresholds.

The entire data base of multiple-pulse thresholds is examined in Part II and an empirical model based on total-on-time is presented. This model is compared to the existing ANSI standard and is seen to give a better overall fit to the experimental data. The additive effects of multiple-pulses are also discussed in terms of the thermal model damage integral.

The project described in Part III of this report is designed to detect visual deficits and to demonstrate the time course of altered visual function following eye insult by laser radiation. This will be accomplished by studying the visual evoked response to phase alternating bar gratings using trained rhesus subjects. The methods being used to train the subjects to observe the viewing area where the gratings will be presented are discussed in detail.

Part IV presents a brief outline of electronics and software being developed for visual stimulus projects being carried out in the Laser Effects Branch, USAF School of Aerospace Medicine.

1

PREFACE

Technical support for the contract was provided by Mr. Gregory L. Sweeney and Mr. Stephen W. Sexauer of Technology Incorporated.

Dr. John Taboada was a collaborator on the helium-cadmium laser work discussed in Part I (Section on "Retinal Damage Induced by UV Laser Exhibiting Self-Mode Locking"). Lt Col William Gibbons and Lt Col William Mikesell cooperated in evaluating retinal damage effects for the multiple-pulse experiments of Part II of this report. All three of these individuals are affiliated with the Laser Effects Branch of the USAF School of Aerospace Medicine (SAM/RZL).

2

TABLE OF CONTENTS

LIST OF FIGURES

LIST OF TABLES

RESEARCH ON THE OCULAR EFFECTS OF LASER RADIATION

PART I

OCULAR EFFECTS OF ULTRAVIOLET LASER RADIATION

Joseph A. Zuclich

INTRODUCTION

An earlier report (1) provided a summary of the UV laser project, including an analysis of experimental threshold data available at the time, and discussions relating the data to a photochemical model, to existing safety standards, and to recommendations for future work. This report deals primarily with two experimental efforts which have been conducted since that time. The first project involves the observation of retinal damage induced by the 325-nm output of a helium-cadmium laser. The retinal threshold occurs at a surprisingly low level despite the absorption of the ocular media at this wavelength. The threshold level may be related to the self-mode-locked nature of the laser output.

The second project deals with the sensitivity of the primate cornea to repeated doses of near-UV radiation. The approach used was to calculate an effective tissue repair rate by determining thresholds for exposures separated by varying intervals from 1 to 48 hours.

Both projects mentioned above have significant implications for protection standards for ocular exposure to near-UV laser radiation. Therefore, an updated discussion of existing safety standards is presented in light of the new experimental data, and appropriate adjustments in the standards are recommended.

RETINAL DAMAGE INDUCED BY UV LASER EXHIBITING SELF-MODE-LOCKING

Previous reports (2,3) discussed the observation of retinal lesions induced in primates (rhesus monkeys) by the UV outputs of krypton- and argon-ion lasers (350-360 nm). However, the occurrence of such lesions proved to be isolated incidents and no combination of exposure parameters was found which reproducibly yielded UV laser-induced retinal damage in test subjects. Nevertheless, the possibility that retinal damage might result from the 325-nm output of helium-cadmium (He-Cd) lasers was recognized because of a small transmission window in the ocular media. This window can be seen in Figure I-1, which shows the percent of corneal incident radiation transmitted to the retina as a function of wavelength.

Two recent studies (4,5) have found corneal and lenticular damage resulting from the UV output of He-Cd lasers. Neither paper mentioned observation of retinal damage effects. The work reported here indicates that retinal damage is induced by 325-nm He-Cd laser radiation at considerably lower energy doses than required to produce either corneal or lenticular
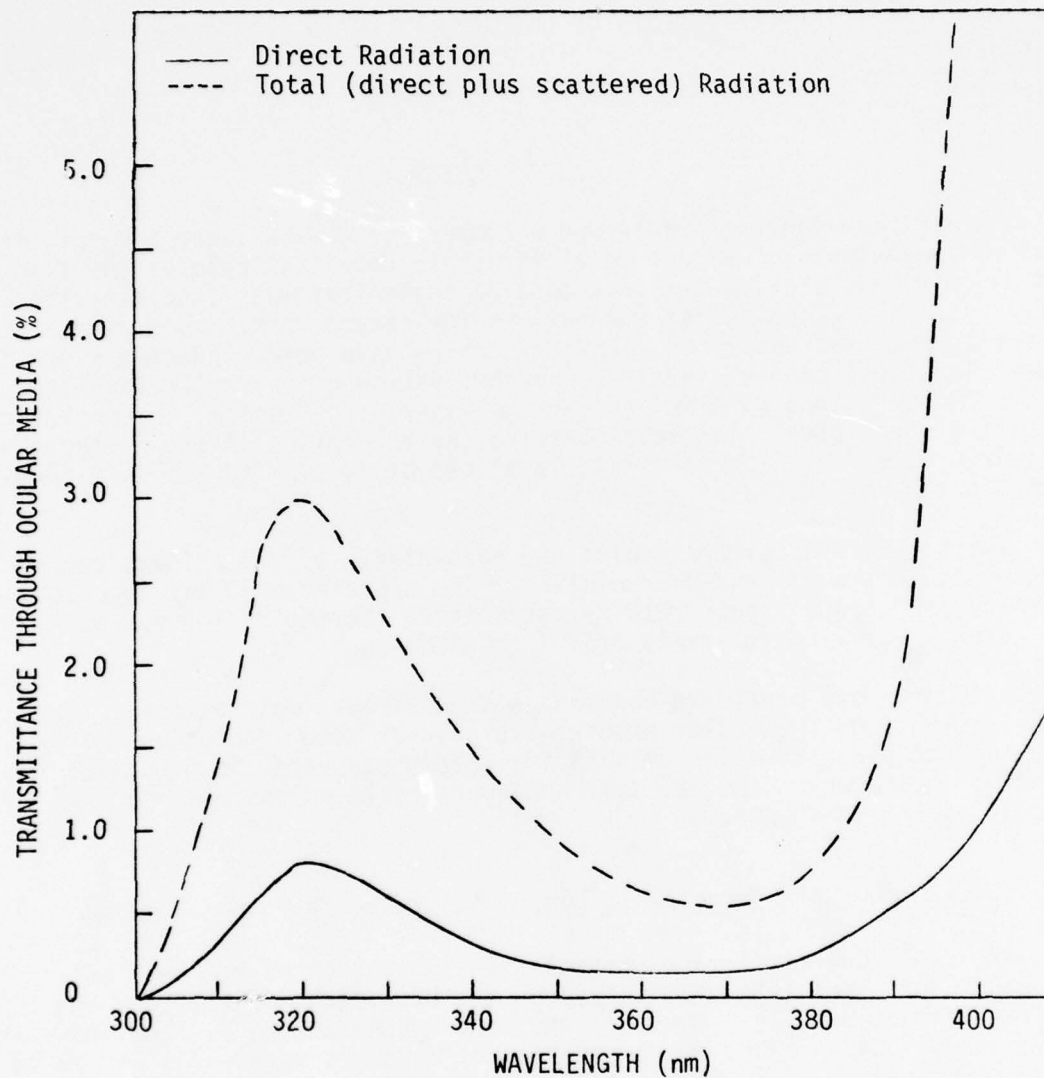
Figure I-1. Transmission spectra of rhesus ocular media $^{(12)}$. Ordinate is percent of corneal incident radiation transmitted to the retina.

8

damage. The unexpectedly low retinal threshold prompted beam diagnostic testing of the He-Cd laser and resulted in the observation of self-mode-locking of the laser output at 325 nm. Self-mode-locking in a He-Cd laser has been previously reported (6) for the 441.6-nm emission, but only mode-locking through intracavity modulation has been reported at 325 nm (7). Two published reports of retinal damage resulting from picosecond pulse trains (8,9) have indicated thresholds low relative to those induced by sources with pulsewidths longer than nanoseconds.

The laser source used in this investigation was a Spectra-Physics 185 helium-cadmium laser with a single isotope (Cd^{114}) tube. The laser output was ∿30 mW at 325 nm. Although several modes and mixed mode outputs could be obtained, the laser mirrors were adjusted to yield maximum output while maintaining the TEM_{00} mode. The resulting beam had a $1/e^2$ diameter of 1.6 mm at the corneal plane of the subjects to be exposed. The beam divergence was 0.5 milliradians. The incident power at the corneal plane was held at ∿20 mW for most exposures, yielding a corneal irradiance of 0.96 W/cm^2. Exposure times were varied with a mechanically triggered electronic shutter to obtain the desired corneal dose.

The experimental subjects were rhesus monkeys, Macaca mulatta. The subjects were tranquilized with an intramuscular injection of ketamine hydro-chloride (10 mg/kg body weight) and anesthetized with sodium pentobarbitol (25-50 mg/kg body weight) introduced into a posterior superficial vein in one leg. Pupil dilation and cycloplegia were induced by atropine admini-stered less than 24 hours prior to the experimental exposures. The eyelid was held open with a wire speculum during exposures, necessitating frequent irrigation with normal saline to prevent corneal desiccation.

Exposure sites were chosen in the macular region of each subject eye with the aid of a Zeiss fundus camera. After the eye was properly posi-tioned, an adjustable mirror mounted on the fundus camera deflected the laser beam onto the desired retinal site. The optical axis of the fundus camera was colinear with the deflected laser beam. As many as sixteen macular sites were exposed in each subject eye, the sites being located at grid points established by paramacular "marker" lesions induced with visible laser radiation several days prior to the UV laser exposures. Marker le-sions were well outside the macular area and had no effect on the subsequent retinal sensitivity to UV laser radiation.

Ophthalmoscopic observations were made at 1 hour and 18-24 hours post exposure, with the 24-hour observations used to determine the thresholds reported here.

Preliminary exposure parameters were chosen to yield corneal doses of the same order of magnitude as the corneal threshold of 32 J/cm^2 previously reported for He-Cd laser radiation (5). This corresponded to an energy of ∿0.8 J delivered to the cornea. It was discovered that such exposures re-producibly yielded retinal lesions which were generally visible immediately following exposure. Initially, the lesions appeared as small white specks which exhibited a high reflectivity. The size of the specks gradually grew, but the reflectivity faded as the lesions developed. Lesion sizes were as great as 300 μm in diameter, with the disrupted areas exhibiting light or bleached central regions surrounded by darkly pigmented rings. Corneal doses of ∿3.0 J/cm^2 or greater resulted in retinal lesions observable

9

immediately following exposure. Energy doses from ~ 0.5 J/cm^2 to ~ 3.0 J/cm^2 generally resulted in minimal lesions appearing within the first hour post exposure. However, by 24 hours post exposure such lesions had developed into distinct pigmented spots 50-100 μm in diameter. Lesions were detected at all exposure sites receiving energy doses of > 0.5 J/cm^2 regardless of the combination of pulsewidth and intensity chosen. Repeated fundus camera observations over a period of several weeks following exposure showed that the lesions did not change appearance during this time. Photographs of representative lesions have been published elsewhere (20).

The criterion chosen for the definition of a threshold retinal lesion was the appearance of a minimal (~ 50 μm) pigmented spot at the exposure site within 24 hours postexposure. The retinal ED_{50} threshold as determined by probit analysis using this criterion was 7.6 $\pm$ 2.3 millijoules. This corresponded to a corneal energy density of 0.36 $\pm$ 0.1 J/cm^2. Dose-response plots and probability curves for the data reported here were included in an earlier report (10).

Corneal and lenticular tissues of exposed eyes were also examined using a Nikon "Zoom-Photo" slit lamp microscope. Lenticular damage was not noted in any of the exposed eyes. Corneal lesions were evaluated at 18-24 hours postexposure in accordance with established criteria (11) for the maximum development of near-UV induced corneal damage. An ED_{50} threshold of 13.7 $\pm$ 0.1 J/cm^2 was obtained compared to an earlier reported value (5) of 32 J/cm^2 for 325-nm He-Cd laser radiation.

The helium-cadmium threshold data is summarized in Table I-1, where it is compared to thresholds for both the UV and visible (blue) outputs of a krypton-ion laser. It is seen that while the He-Cd and krypton-UV corneal thresholds are comparable (allowing for the wavelength dependence of UV-induced corneal damage), the He-Cd retinal threshold is ~ 3 orders of magnitude below that reported for the krypton-UV output. On the other hand, the He-Cd retinal threshold is not too different from previously reported results for visible laser sources, as exemplified by the krypton-blue threshold listed in Table I-1.

At this stage, additional beam diagnostics were initiated to search for an explanation for the anomalously low retinal threshold. Since the direct transmission of the ocular media is less than 1% (Figure I-1) at 325 nm, a small percentage of visible He-Cd output (441.6 nm, where the direct transmission of the ocular media is $\sim 40\%$ (12)) could easily have been responsible for the observed retinal damage. A spectral scan of the laser output with a monochromator, however, ruled out this possibility.

The laser output was next examined with a Spectra Physics 403 high-speed light detector (< 150-psec rise time). The detector was coupled to a Hewlett-Packard 184B high-speed storage oscilloscope with an 1805 amplifier having a 50 Ω input impedance to match the output impedance of the detector. The output of the laser was focused onto the detector surface with a quartz lens. A Gerbrands shutter with a "300 series" digital milli-second timer set for a 5-msec shutter time was used to protect the detector from being overexposed. The supposed cw output of the He-Cd laser appeared to be repetitively pulsed within the temporal resolution of the detection system. The laser output appeared to have a pulse-repetition rate of ~ 10.9 nsec. The rise time and duration seen in the pulses reflect the transfer function

10

TABLE I-1. COMPARISON OF OCULAR THRESHOLDS FROM He-Cd AND KRYPTON-ION LASERS

Laser source	Corneal threshold		Retinal threshold	
	Radiant exposure (J/cm^2)	Energy dose (J)	Radiant exposure (J/cm^2)	Energy dose (J)
Helium-Cadmium-UV (325 nm)	14	0.28	3.6×10^{-1}	7.6×10^{-3} [a]
Krypton-UV (350.7 and 356.4 nm)	67	0.89	> 670	> 8.9
Krypton-blue (476.2 nm)	--	--	4.4×10^{-2}	2.5×10^{-3} [a]

[a] Comparable pulsewidths (350 msec).

11

limitation of the oscilloscope amplifier which had a bandwidth of 100 MHz. The pulse duration can be inferred from Reference 7 to be approximately 900 psec based on the linewidth of the 325-nm emission of Cd^{114}. The intra-cavity round trip transit time ($2L/c$) is approximately 11.7 nsec for a cavity length (L) of 1.76 m, in reasonable agreement with the observed modulation.

Thus, it is concluded that the He-Cd laser exhibits self-mode-locking at 325 nm such as has been previously reported for 441.6 nm (6). However, with no other reports of retinal thresholds due to UV wavelengths currently available for comparison, it is not known if the retinal sensitivity is re-lated to the mode-locked nature of the laser. The threshold value of 0.36 J/cm^2 for 325-nm radiation seems anomalously low when contrasted with the fact that retinal damage is not reproducibly incurred with argon and krypton lasers (350-360 nm) with exposures an order of magnitude or more above the corneal threshold of 67 J/cm^2 (11).

Two additional experiments were contemplated in an attempt to determine if the unexpectedly low retinal threshold reported above is due primarily to enhanced retinal sensitivity to the mode-locked nature of the laser, or if the threshold is representative of a cw source at that particular wave-length. The first experiment (which has already been carried out) was to determine the retinal threshold for the visible output of the He-Cd laser and compare this value to that expected for a non-mode-locked visible wave-length source. Retinal threshold data obtained for the blue (476.2 nm) output from a krypton-ion laser (13) was deemed to be the most appropriate available data for this comparison. The second experiment will be a com-parison of the retinal threshold for 325-nm He-Cd laser radiation to that for a non-mode-locked UV laser source of similar wavelength. An examination of available laser sources has indicated that this can best be accomplished with the 333.6-nm radiation which constitutes approximately 5% (40 mW) of the UV output of a Spectra-Physics 170 argon-ion laser. The 333.6-nm output will have to be selected while filtering out the argon-laser emissions at 351.1 and 363.8 nm.

The results of the retinal threshold determination using the 441.6-nm He-Cd output were inconclusive. The visible output did not exhibit as "clean" a mode-locked structure as the UV output. The amplitude of the mode-locked output varied significantly with time and at certain instances represented only a small modulation on the steady cw output. For the re-tinal threshold determination, a 40-msec pulsewidth was chosen to allow direct comparison with data collected using the 476.2-nm output of a krypton-ion laser (13). The retinal threshold for 40-msec exposures was ~13 mW (0.52 mJ) incident at the cornea. This compares with the krypton laser threshold of ~12 mW (0.48 mJ). Thus, the partial mode-locking that is ob-served with the visible output of the He-Cd laser does not significantly alter the retinal sensitivity for these exposure conditions. The lesions induced by the 441.6-nm output had the appearance expected for thermally induced retinal damage and did not exhibit the dark pigmentation associated with the UV-induced retinal lesions.

The nature of the dark pigmentation formed as a result of the He-Cd UV laser exposures and its location within the retinal layers are currently unknown, but histopathologic evaluation of retinal tissues subjected to sub- and suprathreshold doses of 325-nm laser radiation is currently under way.

12

A preliminary verbal report of the histopathologic results has indicated that damage is most pronounced in the photoreceptors, with necrosis of photoreceptor inner segments and pyknosis or loss of adjacent nuclei in the outer nuclear layer. Unlike lesions induced by visible laser radiation, the retinal pigment epithelium appears to be unaffected.

REPAIR OF UV LASER-INDUCED CORNEAL DAMAGE

Studies by Technology Incorporated for the Laser Effects Branch (USAFSAM) have indicated that corneal damage induced by near-UV laser radiation is the result of a photochemical damage mechanism (11). Thus, a reciprocity relationship exists between the laser intensity and exposure time such that the same total energy dose is required to reach the damage endpoint (i.e., observation of a visible lesion) for varying combinations of these two parameters. Another obvious consequence of a single-photon photochemical mechanism is that the effects of repeated exposures will be cumulative provided only that there is no repair or replacement of the damaged tissue during the time between exposures. A comprehensive safety standard for the safe use of UV lasers should, therefore, include specification of the period of time over which UV exposures would be regarded as cumulative. Unfortunately, no quantitative guidelines for such a specification have appeared in the literature.

Slit-lamp observations of UV laser-induced corneal lesions indicate that the degree of observable damage develops gradually over a period of from 12 to 24 hours following the exposure (11). The damage, if restricted to the epithelial layer, appears to completely repair within 48 to 72 hours postexposure. Based on these observations and an earlier study on ocular effects of noncoherent UV radiation (14), it seems prudent to assume that the effect of UV radiation on corneal tissue will be cumulative over a period of 24 hours or longer. The experiment described below was designed in order to obtain a quantitative evaluation of the cumulative nature of UV-induced corneal damage. A major objective of this project is to determine an effective tissue repair rate to be incorporated into a quantitative photochemical model so that reliable threshold predictions can be made for long exposures or repeated exposures over periods of hours to days.

An effective tissue repair rate for UV-induced corneal damage was obtained by determining corneal thresholds for two identical exposures spaced at varying intervals ranging from 1 hour to 48 hours. The laser source chosen was a Coherent Radiation 500K krypton-ion laser equipped with mirrors to yield UV output at 350.7 and 356.4 nm simultaneously. The maximum UV output of the laser was ∼100 mW, but the emission tended to be multi-mode unless the laser tube current was reduced to the point that only a fraction of this power was obtained. To maximize the UV output while maintaining the TEM_{00} mode, an intracavity aperture (1.5 mm diameter) was mounted between the rear Brewster window and rear mirror. In this way, an output of ∼40 mW was obtained in the TEM_{00} mode.

The success of this experiment required precise placement of the UV beam so that substantially the same corneal tissue was irradiated during each exposure. The usual technique of positioning the subject eye with the aid of a He-Ne alignment laser (3) was not deemed accurate enough for this purpose. Rather, the subjects were mounted in position for viewing with a Zeiss fundus camera (in the same way as subjects to be exposed for retinal

13

damage studies). The fundus camera was focused on the anterior ocular tissue so that the pupil was centered in the field of view. The fundus camera reticle was used as a reference to reproducibly position the subject pupil with respect to the reticle crosshairs. In order to achieve more precise centering, the pupils were not dilated. Thus, the pupil size was only slightly larger than the beam spot size incident at the cornea and during the exposures it could be verified that the irradiated corneal tissue was centered directly over the pupil without any of the iris tissue being irradiated.

The UV beam was deflected onto the cornea by an adjustable mirror mounted on the fundus camera. The experimental procedure was the same as used for retinal laser exposures, as can be seen from the block diagram of the apparatus shown in Figure I-2. Animal handling procedures were as described on page 9 of this report.

Initial experiments consisted of single-pulse exposures in order to establish agreement with previously reported krypton laser thresholds (11). The beam spot size measured at the corneal plane was ∿1.75 mm, $1/e^2$ diameter. The power incident at the cornea was typically about 30 mW. Exposure time was varied in order to obtain the corneal threshold. Under these conditions, an exposure time of ∿40 sec was required to induce a corneal lesion. The calculated threshold dose was 55.3 J/cm^2 with 95% confidence limits of 46.9 and 64.5 J/cm^2, compared to a threshold of 62 J/cm^2 previously determined for 45-sec exposures (11).

The corneal threshold was next determined for two identical exposures delivered at an interval of one hour. The power level was held constant for all exposures. The durations of the two exposures delivered to the same eye were equal, but the exposure times were varied from eye to eye. The corneal threshold for two exposures was found to be 55.8 J/cm^2, in close agreement with the single-pulse threshold. Thus, whereas a single 40-sec exposure was previously found to induce a minimal corneal lesion, two 20-sec exposures separated by 1 hour (all other exposure parameters being held constant) produced the same effect. This indicates that there is no effective repair of corneal tissue over a period of 1 hour and that the effects of multiple exposures delivered within a 1-hour period would be additive.

The equivalence of the single- and double-pulse thresholds quoted above illustrates the precision of the technique used for assuring that the same patch of corneal tissue was irradiated whenever a given eye received more than one exposure. After establishing the validity of the technique, experiments then continued for exposures separated by intervals between 6 and 48 hours. In particular, thresholds were determined for exposure separations of 6, 18, 30 and 48 hours. The results are summarized in Table I-2. Dose-response plots for each of the threshold determinations are collected in the Appendix.

The corneal threshold is shown plotted as a function of pulse separation in Figure I-3. Tissue repair following the initial exposure would not be complete until the threshold for two separated exposures approaches twice the single-pulse threshold. Repair within a 24-hour period is minimal (Figure I-3). There is some cumulative effect even for times up to 48 hours and according to the extrapolation indicated in Figure I-3, recovery would not be complete until ∿72 hours following the initial insult. To verify this,

14
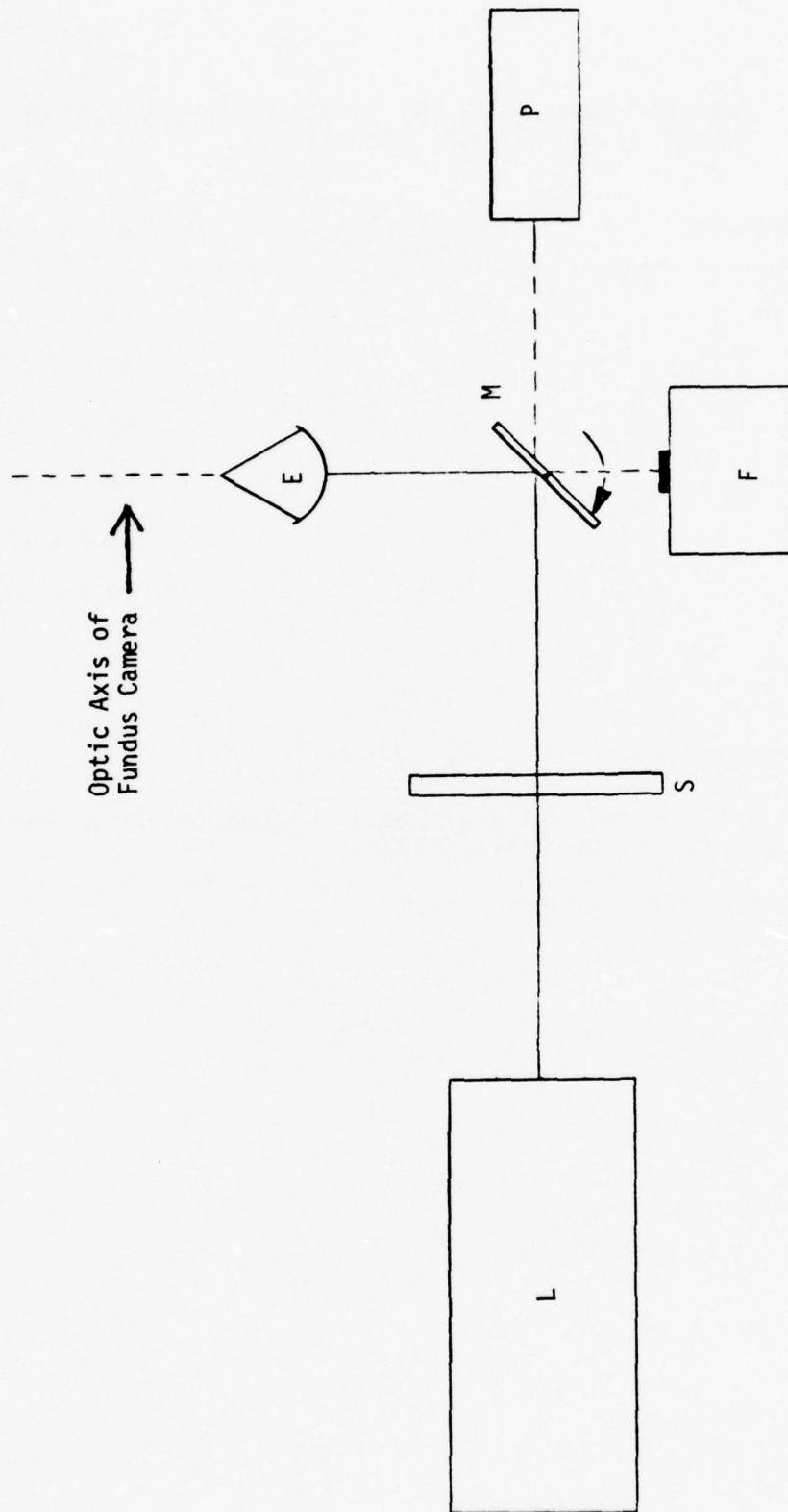
Figure I-2. Experimental apparatus for inducing UV corneal lesions.
L – Coherent Radiation 500K krypton-ion laser
S – electronically triggered mechanical shutter
E – subject eye
M – swinging mirror attached to fundus camera
F – fundus camera
P – laser power meter

TABLE I-2. THRESHOLD IRRADIANCES FOR CORNEAL EPITHELIAL LESIONS
INDUCED BY TWO UV LASER EXPOSURES[a]

Time between exposures (hours)	Threshold[b] (J/cm^2)	95% Confidence limits (J/cm^2)
Single pulse	55.3	46.9 - 64.5
1	55.8	47.5 - 65.5
6	60.5	60.2 - 60.8
18	64.1	56.8 - 72.2
30	68.2	63.2 - 73.5
48	84.7	79.1 - 90.6

---

[a] Subjects received two identical exposures to krypton-ion laser (350.7 and
356.4 nm) separated by the indicated times.

[b] Total energy dose from two exposures.
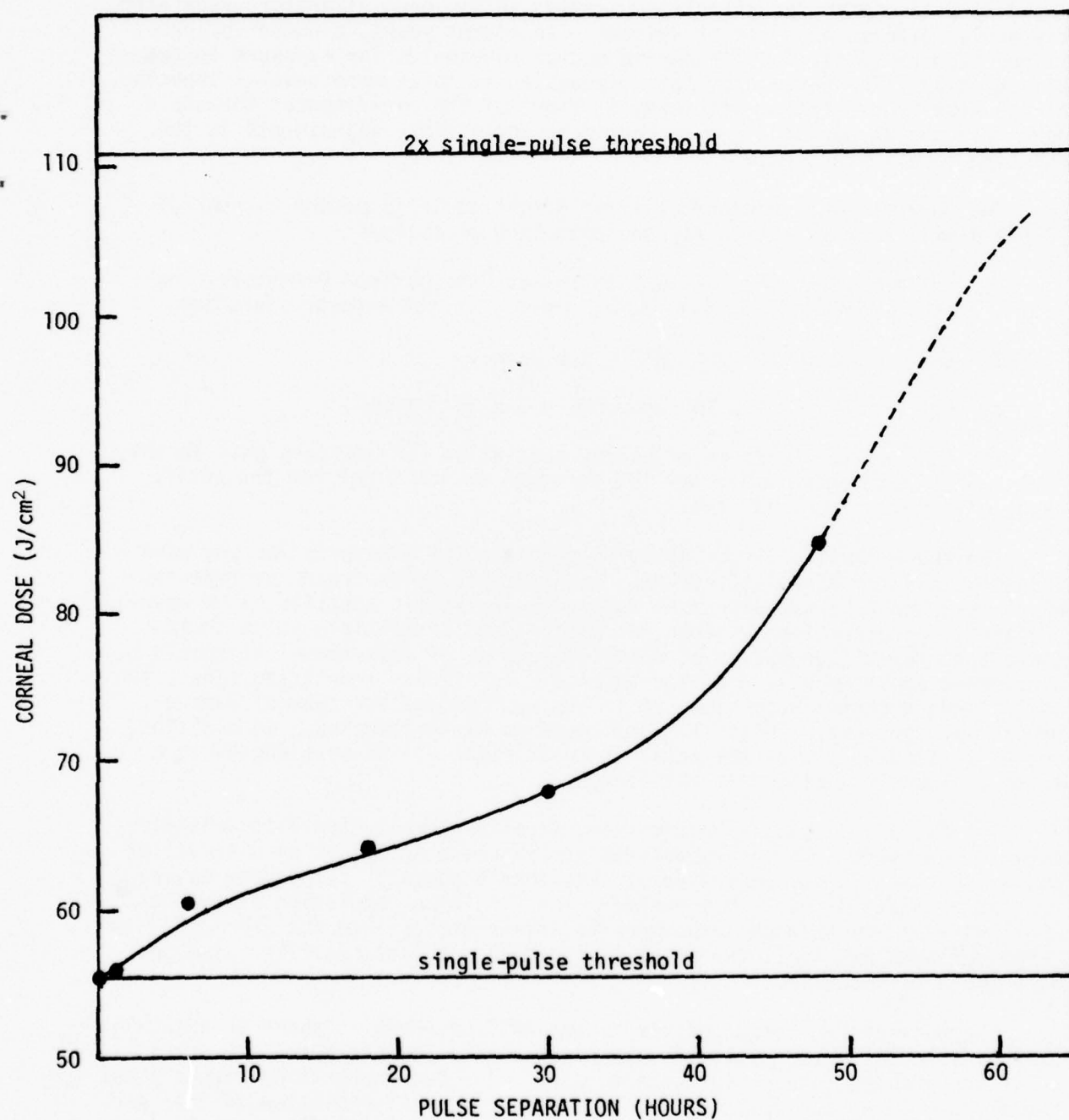
Figure I-3. Corneal thresholds for exposures to two identical UV laser pulses with varying interpulse separation. The solid curve is a smooth-line empirical fit.

17

threshold determinations will continue for exposures separated by 72 hours and longer, if necessary.

PROTECTION STANDARDS FOR OCULAR EXPOSURE TO NEAR-UV LASER RADIATION

Existing safety standards for the safe use of lasers (15,16) were formulated at a time when few guidelines existed in the open literature regarding the ocular effects of UV laser systems. In recent years, a number of published studies (5,11,17-20) reported ocular thresholds for exposure to near-UV radiation. The purpose of this discussion is to examine several aspects of the near-UV protection standards in light of the experimental threshold data that has accumulated and to recommend appropriate adjustments in the existing safety standards.

The current ANSI standard (15) for direct ocular exposure to near-UV (315-400 nm) laser radiation may be summarized as follows:

1) For exposure times of 10^{-9} to 10 sec, the maximum permissible exposure (MPE) is $0.56\tau^{\frac{1}{4}}$ J/cm^2, where τ is the exposure duration.

2) For τ = 10 to 10^3 sec, MPE = 1.0 J/cm^2.

3) For τ = 10^3 to 3 x 10^4 sec, MPE = 1 x 10^{-3} W/cm^2.

The current Air Force laser safety regulation (16) differs only in the long pulsewidth regime where the MPE is equal to 1.0 J/cm^2 for the entire range of τ = 10 to 10^4 sec.

The above considerations apply to single-pulse exposures for any wavelength within the range 315-400 nm. For multiple-pulse trains or repeated exposures, the ANSI standard does not quote any limits specific to UV wavelengths. The general provisions for visible and IR multiple-pulse trains state that repetitive pulses at repetition rates of less than 1 Hz should be considered additive over a 24-hour period. For higher repetition rates, the ANSI standard quotes provisions which are appropriate for thermal damage mechanisms, but not necessarily applicable to UV wavelengths. In addition, the ANSI standard limits the total irradiance for all UV wavelengths to a value of 1 W/cm^2 incident at the cornea.

The Air Force regulation does specifically address itself to multiple-pulse UV exposures, which are defined as "exposure to pulses of ultraviolet radiation (λ < 400 nm) separated by less than 8 hours." The exposures are treated as additive over this period. The Air Force regulation stipulates additivity of simultaneous exposures to wavelengths within the 200-to 400-nm range but does not limit the total UV irradiance to any specific value, as does the ANSI standard.

The near-UV MPE curve defined by the ANSI standard is shown as a log-log plot of irradiance vs. pulsewidth in Figure I-4. The Air Force MPE curve coincides with the ANSI curve except for $\tau > 10^3$ sec where it continues along the 1 J/cm^2 level as indicated by the dotted line. Also plotted on the same figure are numerous ED$_{50}$ thresholds for near-UV-induced corneal epithelial lesions. The ED$_{50}$ threshold data shown are summarized in Tables I-3 and I-4. Table I-3 lists the results of single-pulse exposures while Table I-4 includes available multiple-pulse exposure data.

18
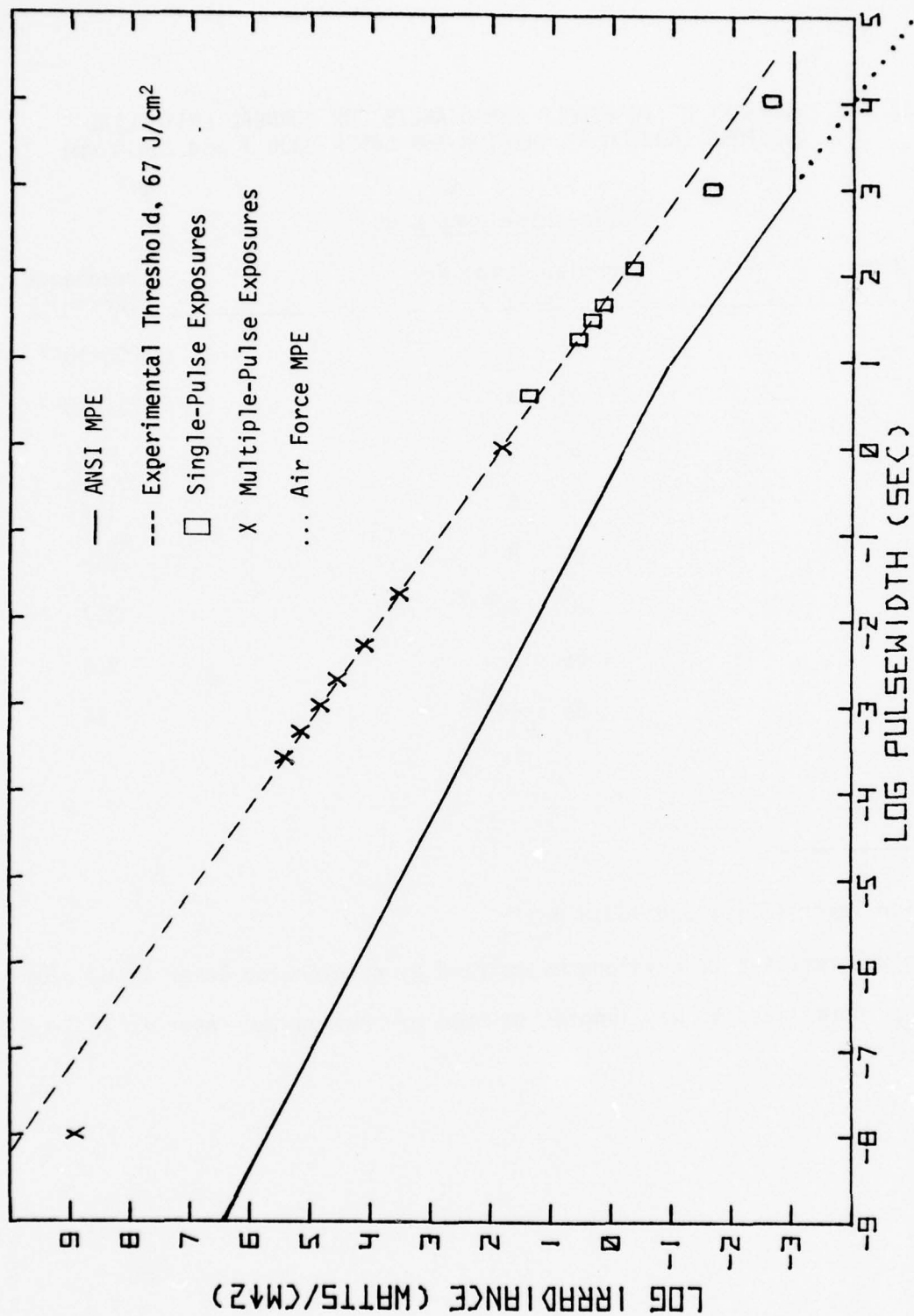
Figure I-4. Comparison of experimentally determined corneal thresholds with present ANSI maximum permissible exposures for 315- to 400-nm radiation.

TABLE I-3. SUMMARY OF THRESHOLD IRRADIANCES FOR CORNEAL EPITHELIAL
LESIONS INDUCED BY KRYPTON-ION LASER (350.7 and 356.4 nm)

Single-pulse exposures

Exposure time (sec)	Radiant exposure (J/cm^2)	Irradiance (W/cm^2)
10^4	26 ± 1	2.6×10^{-3}
10^3	21 ± 4	2.1×10^{-2}
120	53 ± 8	0.44
45	62 ± 6	1.4
30	66 ± 8	2.2
30	82 ± 23[a,b]	2.7
18	66 ± 8	3.6
4	96 ± 14[a,c]	24

---

[a] Argon-ion laser (351.1 and 363.8 nm).

[b] Threshold normalized to wavelengths emitted by krypton-ion laser is 67 J/cm^2.

[c] Threshold normalized to wavelengths emitted by krypton-ion laser is 79 J/cm^2.

TABLE I-4. SUMMARY OF THRESHOLD IRRADIANCES FOR CORNEAL EPITHELIAL
LESIONS INDUCED BY KRYPTON-ION LASER (350.7 and 356.4 nm)

Multiple-pulse exposures
(30-sec pulse trains, 50% duty cycle)

Pulsewidth (msec)	Radiant exposure (J/cm^2)	Irradiance (Per pulse) (W/cm^2)	Number of pulses	Calculated irradiance for threshold dose delivered in single-pulse (W/cm^2)
10^3	66 ± 9	4.4	15	66
20	67 ± 6	4.4	7.5×10^2	3.3×10^2
5	63 ± 10	4.2	3×10^3	1.3×10^4
2	71 ± 15	4.8	7.5×10^3	3.6×10^4
1	67 ± 12	4.5	1.5×10^4	6.8×10^4
0.5	71 ± 10	4.7	3×10^4	1.4×10^5
0.25	64 ± 12	4.3	6×10^4	2.6×10^5
10^{-5}[a]	8.4 ± 3.3[b]	1.1×10^8	8[c]	8.8×10^8

---

[a] Duty cycle, 10^{-7}.

[b] Nitrogen laser (337.1 nm).

[c] Pulse train length, 0.8 sec.

With the exception of the extreme pulsewidths (10^{-8}-sec nitrogen laser threshold and 10^3- and 10^4-sec krypton laser thresholds) the data fall very close to a straight line representing an energy dose of 67 J/cm^2 delivered to the cornea. This value is represented by the dashed line shown in Figure I-4. The two thresholds determined with argon-laser radiation fall at a slightly higher value due to the wavelength dependence of UV-induced corneal damage which is discussed below.

The fact that the product of threshold intensity and pulsewidth is essentially constant (reciprocity relationship) from $\lesssim 10^{-4}$ sec to $\gtrsim 10^2$ sec supports the postulate that the epithelial damage mechanism involves a single-photon photochemical process (11,17,18). It should also be noted that the thresholds for multiple-pulse exposures are in agreement with those for single-pulse exposures, clearly demonstrating the cumulative effect of repetitive pulses and thereby providing further support for the hypothesis of a photochemical mechanism. These results support the additive treatment of multiple-pulse or repeated exposures to UV-laser radiation.

The MPE for $\tau < 10$ sec ($0.56 \, \tau^{1/4}$ J/cm^2) appears to reflect the assumption of a thermal damage mechanism and might be considerably more restrictive than necessary for shorter pulsewidths. For example, as seen in Figure I-4, the MPE for 10^{-8} sec is $\sim$3 orders of magnitude less than the corneal threshold observed with 10-nsec nitrogen laser pulses (337.1 nm). On the other hand, it is only $\sim$2 orders of magnitude below the threshold for immediate cataract formation (17), with the threshold for long-term cataract formation yet to be determined. Further, the nitrogen laser corneal and lenticular thresholds are the only near-UV threshold data available in the nsec - μsec pulsewidth range. Therefore, it would seem to be premature to suggest relaxation of the near-UV MPE for shorter pulsewidths although such an action may eventually prove desirable.

The MPE of 1 J/cm^2 for 10 - 10^3 sec appears to be acceptable for the near-UV wavelength range. The data plotted in Figure I-4 indicate that the threshold irradiance-pulsewidth reciprocity continues to hold for exposure durations as long as 10^4 sec. Therefore, it seems appropriate to have the MPE continue to follow the 1 J/cm^2 curve for $\tau > 10^3$ sec. In this regard, the current Air Force regulation seems more suitable than the 1976 ANSI standard.

Related to the question of validity of the reciprocity relationship for long exposure durations is the treatment of multiple-pulse or repeated exposures over long periods of time. As mentioned above, the ANSI standard does not address itself to multiple-pulse UV exposures, while the Air Force regulation treats UV exposures as additive over an eight-hour period. Since the development of UV-induced corneal epithelial lesions as monitored by slit lamp observations is not completed until 12-24 hours postexposure, and the corneal disruption may still be observable with the slit lamp for up to 48 hours or more postexposure (11,17), it seems likely that cumulative effects of repeated exposures would be found for periods in excess of 8 hours. To demonstrate this, the experiment reported on page 13 was carried out to obtain a quantitative evaluation of the cumulative nature of UV-induced corneal damage. The effective tissue repair rate for UV-induced damage was examined by measuring corneal thresholds for two identical UV-laser exposures spaced at varying intervals from 1-48 hours. As can be seen from Table I-2 and Figure I-3, repair within a 24-hour period is minimal, and there is some

22

cumulative effect up to times of $\sim$72 hours following the initial exposure. Thus, a moderately conservative safety standard should treat the effects of repeated UV exposures as additive over a 72-hour period with the MPE for such a period restricted to the MPE for long single-pulse exposures of the appropriate wavelength (i.e., 1 J/cm^2 for 315-400-nm radiation). For personnel who could be exposed to UV radiation on a daily basis, the MPE for any 24-hour period should be no more than one-third of the single-pulse MPE.

The experimental threshold curve (dashed line) shown in Figure I-4 represents the best fit to threshold data determined using the UV output of a krypton-ion laser (350.7 and 356.4 nm; intensity ratio 3:1). Threshold irradiance vs. pulsewidth curves for other UV wavelengths are expected to be parallel to the line drawn in Figure I-4, but the threshold energy varies significantly over the wavelength range of 315 to 400 nm. This wavelength dependence is illustrated by the near-UV corneal threshold data summarized in Table I-5 and plotted in Figure I-5. Because the corneal threshold varies by approximately two orders of magnitude from 315 to 400 nm, it is difficult to quote an MPE which provides an adequate margin of safety for all exposure parameters without being unnecessarily restrictive in certain instances. Therefore, it may be desirable to divide the 315-400-nm wavelength range into two or more segments and to quote an appropriate MPE for each region. However, for wavelengths in the vicinity of 400 nm, the threshold for retinal damage is likely to be comparable to or possibly lower than that for corneal damage, and the MPE should be determined on the basis of potential retinal hazard. At the present time, the author is not aware of any retinal threshold determinations for wavelengths between $\sim$360 and 440 nm.

Several instances of lenticular and retinal damage from near-UV laser radiation have been discussed in the literature (11,17,20). At the present time, the only case which would appear to impact upon the MPE levels for near-UV radiation involves the observation of retinal damage induced by 325-nm radiation from a helium-cadmium laser (see page 7). In this case, the threshold for retinal damage not only is much lower than the corneal threshold, but is also below the MPE's quoted in the current ANSI standard and Air Force regulation. However, this assumes that the He-Cd laser is a cw source. As shown on page 7 and in Reference 20, the He-Cd laser used was found to exhibit self-mode-locking so that the output actually consisted of trains of ultra-short pulses spaced at intervals of $\sim$11 nsec. Although the pulsewidth was not measured directly, it can be inferred (7,20) to be $\sim$900 psec based on the linewidth of the 325-nm emission of Cd[114]. If the He-Cd laser is treated as a pulsed source with a pulsewidth of $\sim$1 nsec rather than as a cw source, the MPE would be $\sim$3 mJ/cm^2 which provides an adequate margin of safety relative to the experimental threshold. Therefore, a provision must be included in the safety standards to the effect that any seeming cw source which belongs to a family of lasers known to exhibit spontaneous mode-locking (9,21) (whether a pure mode-locked output or a pulsed output superimposed on a cw background) must be treated as a pulsed source. Similarly, any pulsed laser source which actually has pulse substructure due to self-mode-locking must be treated as a source having the ultrashort pulsewidth associated with the mode-locking.

23

TABLE I-5. WAVELENGTH DEPENDENCE OF THRESHOLDS (ED_{50}) FOR CORNEAL LESIONS
INDUCED BY NONCOHERENT NEAR-UV RADIATION

Wavelength [a] (nm)	No. of eyes	Threshold (J/cm^2)	95% Confidence limits (J/cm^2)
320	22	9.6	8.5 - 10.7
330	27	41.1	35.3 - 47.7
340	33	58.3	51.6 - 65.8
350	26	61.5	55.0 - 68.5
360	24	88.4	b
370	25	130	116 - 147
380	25	179	157 - 205
390	29	258	230 - 288

[a] 10-nm bandwidth.

[b] No overlap of "Lesion" and "No Lesion" data.
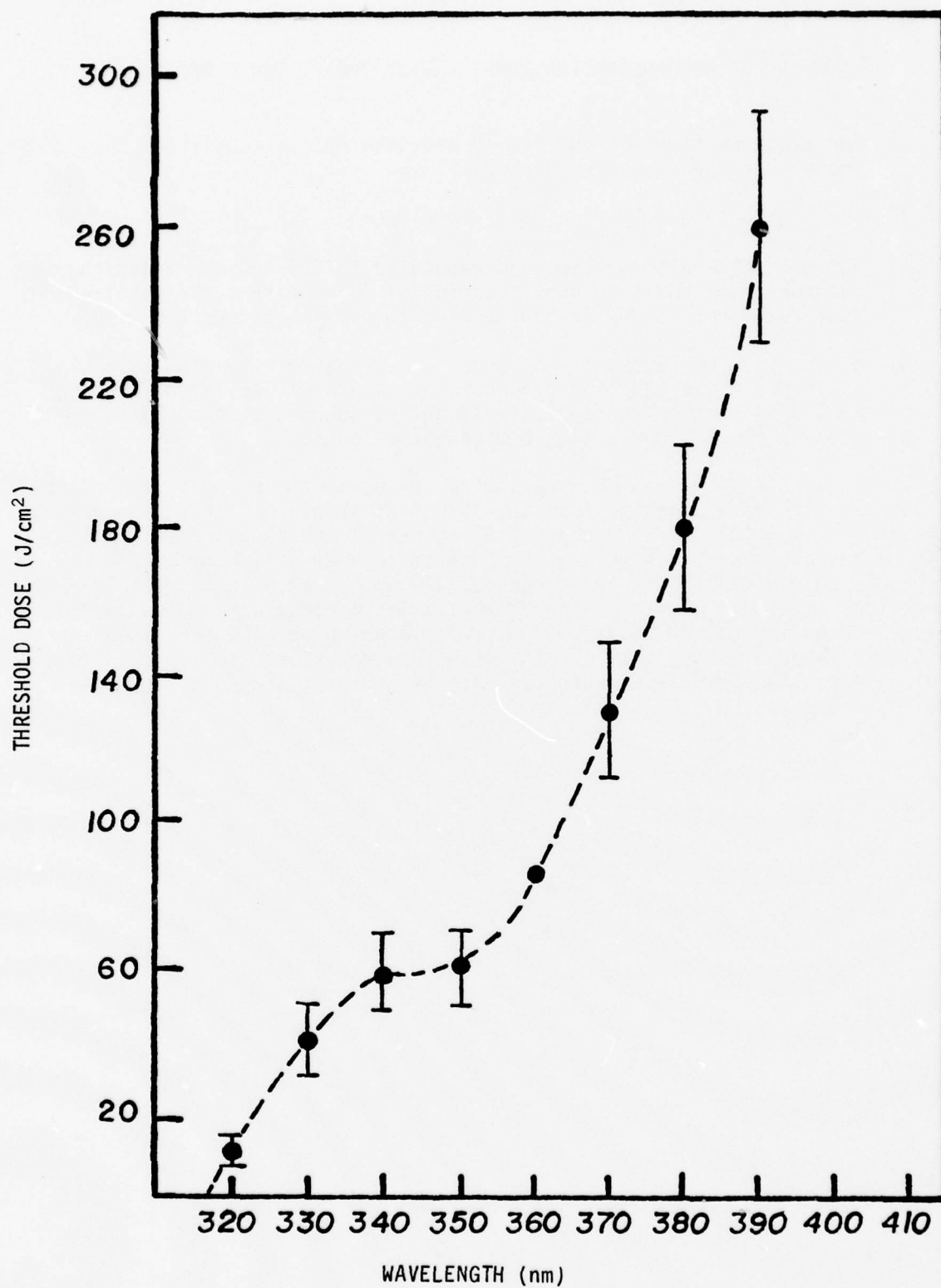
Figure I-5. Experimental thresholds for corneal epithelial lesions induced by monochromatic, noncoherent near-UV radiation.

25

SUMMARY OF RECOMMENDATIONS FOR NEAR-UV PROTECTION STANDARD

1) For exposure times of 10^{-9} to 10 sec, the MPE is equal to $0.56\tau^{\frac{1}{4}}$ J/cm^2 where τ is the exposure duration.

2) For $\tau = 10$ to 3×10^4 sec, MPE = 1.0 J/cm^2.

3) For multiple-pulse or repeated exposures to 315-400-nm radiation, the exposures are additive over a period of 72 hours and the total energy dose delivered in any 72-hour period should not exceed 1.0 J/cm^2.

4) Helium-cadmium lasers or any other laser source belonging to a class of lasers which has been demonstrated to exhibit self-mode-locking should be treated as repetitively-pulsed sources with the MPE limited to the MPE for a single mode-locked pulse.

Items 1 and 2 above are in accord with the current Air Force regulation, but item 2 represents a change from the 1976 ANSI standard. Item 3 represents a change from both the Air Force and ANSI standards and is based on the tissue repair rate data reported herein. The additivity over a 72-hour period may also apply to wavelengths in the range 200-315 nm. Item 4 is based solely on the retinal threshold observed with 325-nm radiation from a He-Cd cw laser. Helium-neon cw lasers and Nd:YAG, Q-switched lasers have also been shown to exhibit self-mode-locking (21) and the same considerations should apply to a wavelength doubled (316.4-nm) output from a He-Ne laser, or to a frequency tripled (353.3-nm) Nd:YAG output.

REFERENCES

1. Zuclich, J. A. In Research on the ocular effects of laser radiation. Technology Incorporated, Quarterly Report 1, Part I, Contract F33615-77-C-0615, USAF School of Aerospace Medicine, June 1977.

2. Sanders, V. E., and J. A. Zuclich. Research on the eye effects of laser radiation. Technology Incorporated, First Annual Report, Contract F41609-73-C-0017, USAF School of Aerospace Medicine, Feb 1974.

3. Zuclich, J. A., et al. In Research on the eye effects of laser radiation. Technology Incorporated, Second Annual Report, Part II, Contract F41609-73-C-0017, USAF School of Aerospace Medicine, Feb 1975.

4. MacKeen, D., S. Fine, and B. S. Fine. Production of cataracts in rabbits with the ultraviolet laser. Ophthal Res 5:317 (1973).

5. Ebbers, R. W., and D. Sears. Ocular effects of 325 nm ultraviolet laser. Am J Optom Physiol Opt 52:216 (1975).

6. Faxvog, F. R., G. W. Willenbring, and J. A. Carruthers. Self-pulsing in the He-Cd laser. Appl Phys Letters 16:8 (1970).

7. Silfvast, W. T., and P. W. Smith. Mode-locking of the He-Cd laser at 4416 and 3250 Å. Appl Phys Letters 17:70 (1970).

8. Smart, D., et al. New ocular hazard of mode locking in cw laser. Nature 227:1149 (1970).

9. Taboada, J., and R. W. Ebbers. Ocular tissue damage due to ultrashort 1060-nm light pulses from a mode-locked Nd:glass laser. Appl Opt 14:1759 (1975).

10. Zuclich, J. A. In Research on the ocular effects of laser radiation. Technology Incorporated, Quarterly Report 3, Part I, Contract F33615-77-C-0615, USAF School of Aerospace Medicine, Dec 1977.

11. Zuclich, J. A., and J. S. Connolly. Ocular damage induced by near-ultraviolet laser radiation. Invest Ophthalmol 15:760 (1976).

12. Boettner, E. A. Spectral transmission of the eye. University of Michigan, Final Report, Contract AF 41(609)-2966, USAF School of Aerospace Medicine, July 1967.

13. Sanders, V. E. Research on the eye effects of laser radiation. Technology Incorporated, Quarterly Report Number 2, Contract F41609-73-C-0017, USAF School of Aerospace Medicine, Aug 1973.

14. Verhoeff, F. H., L. Bell, and C. B. Walker. The pathologic effects of radiant energy on the eye. Proc Am Acad Arts Sci 51:630 (1916).

15. American National Standard for the Safe Use of Lasers. Standard Z136.1, American National Standards Institute, 1976.

16. Laser Health Hazards Control. Revised AFR 161-32.

17. Zuclich, J. A., et al. <u>In</u> Research on the ocular effects of laser radi-
    ation. Technology Incorporated, Final Report, Contract F41609-73-C-0017,
    USAF School of Aerospace Medicine, Aug 1977.

18. Zuclich, J. A., and W. E. Kurtin. Oxygen dependence of near-ultraviolet
    induced corneal damage. Photochem Photobiol 25:133 (1977).

19. Kurtin, W. E., and J. A. Zuclich. Action spectrum for oxygen-dependent
    near-ultraviolet induced corneal damage. Photochem Photobiol 27:329
    (1978).

20. Zuclich, J. A., and J. Taboada. Ocular hazard from UV laser exhibiting
    self-mode-locking. Appl Opt 17:1482 (1978).

21. Taboada, J. Picosecond pulses due to self-mode-locking in lasers.
    SAM-TR-74-47, Nov 1974.

APPENDIX I-A

DOSE-RESPONSE PLOTS

Figure I-A-1. Dose-response plot for corneal damage induced by single-pulse exposures to krypton-ion laser. (350.7 and 356.4 nm; corneal spot size 1.7-mm diameter.)

PROBABILITY OF DAMAGE (%)

100

75

50

25

0

20.0 30.5 41.1 51.6 62.1 72.7 83.2 93.7

CORNEAL DOSE (J/CM↑2)

LESION

NO LESION

Figure I-A-2. Dose-response plot for corneal damage induced by two exposures to krypton-ion laser. (350.7 and 356.4 nm; corneal spot size 1.7-mm diameter; exposures separated by 1-hour intervals.)

31

Figure I-A-3. Dose-response plot for corneal damage induced by two exposures to krypton-ion laser. (350.7 and 356.4 nm; corneal spot size 1.7-mm diameter; exposures separated by 6-hour intervals.)

Figure I-A-4. Dose-response plot for corneal damage induced by two exposures to krypton-ion laser. (350.7 and 356.4 nm; corneal spot size 1.7-mm diameter; exposures separated by 18-hour intervals.)

33
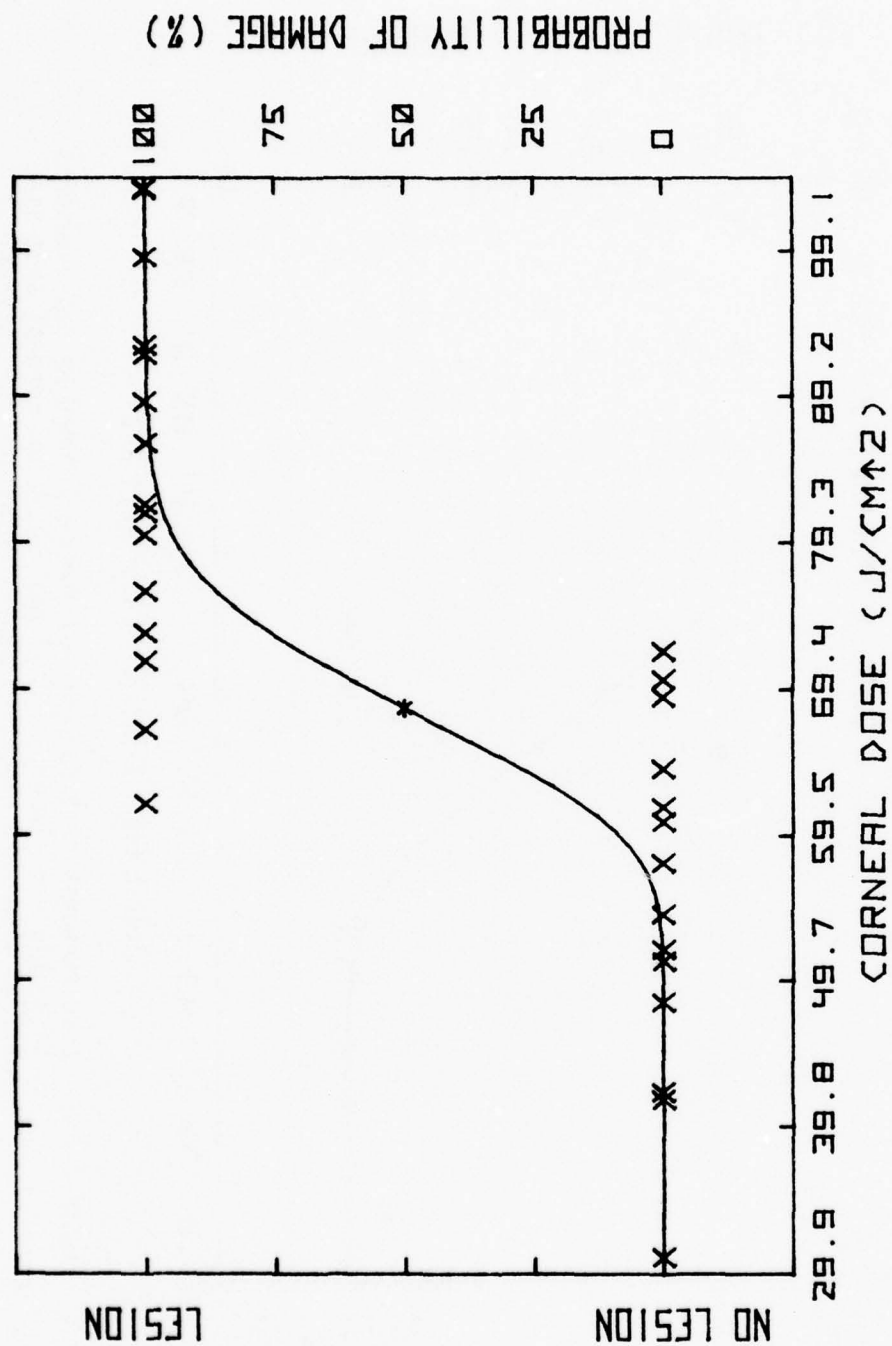
Figure I-A-5. Dose-response plot for corneal damage induced by two exposures to krypton-ion laser. (350.7 and 356.4 nm; corneal spot size 1.7-mm diameter; exposures separated by 30-hour intervals.)
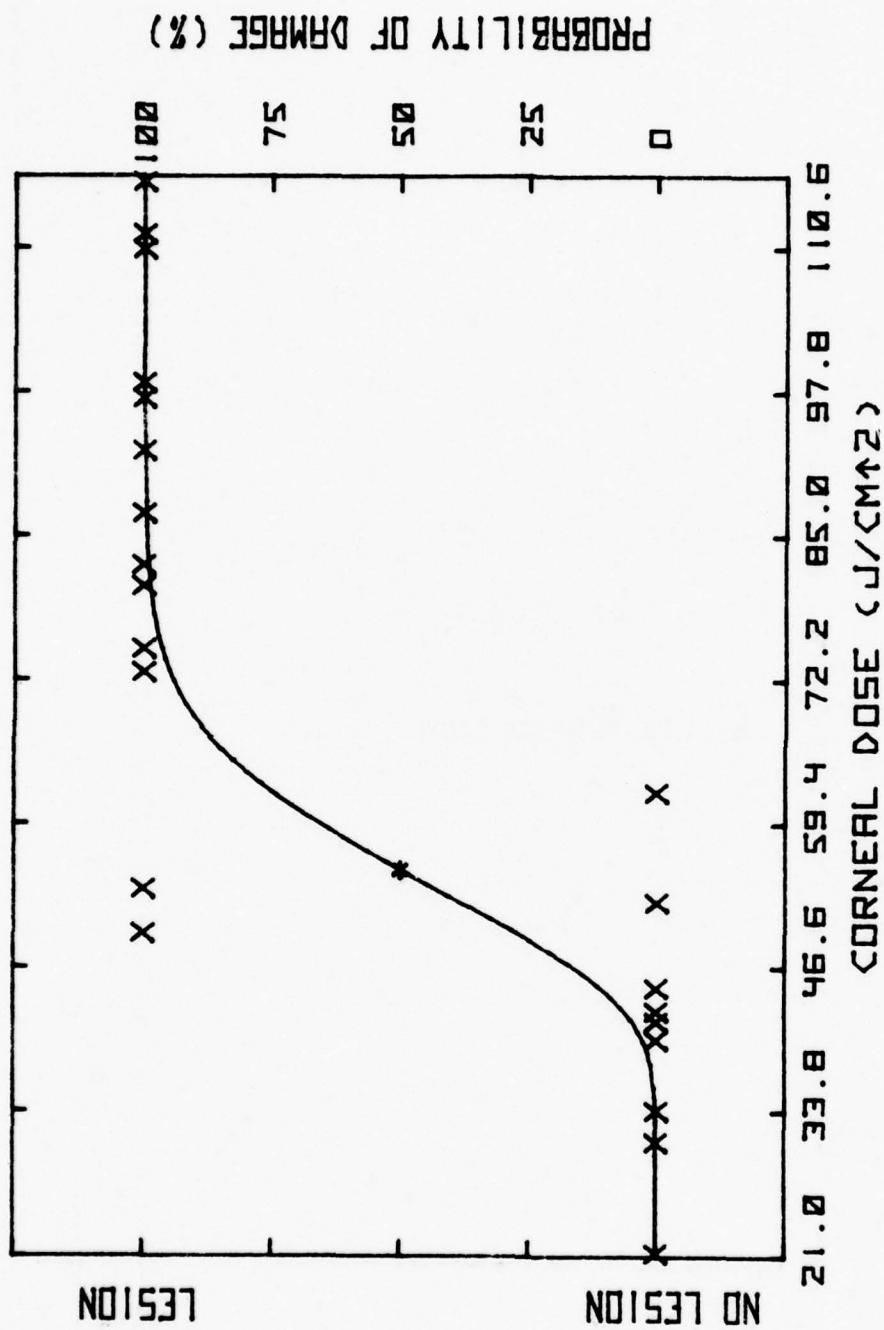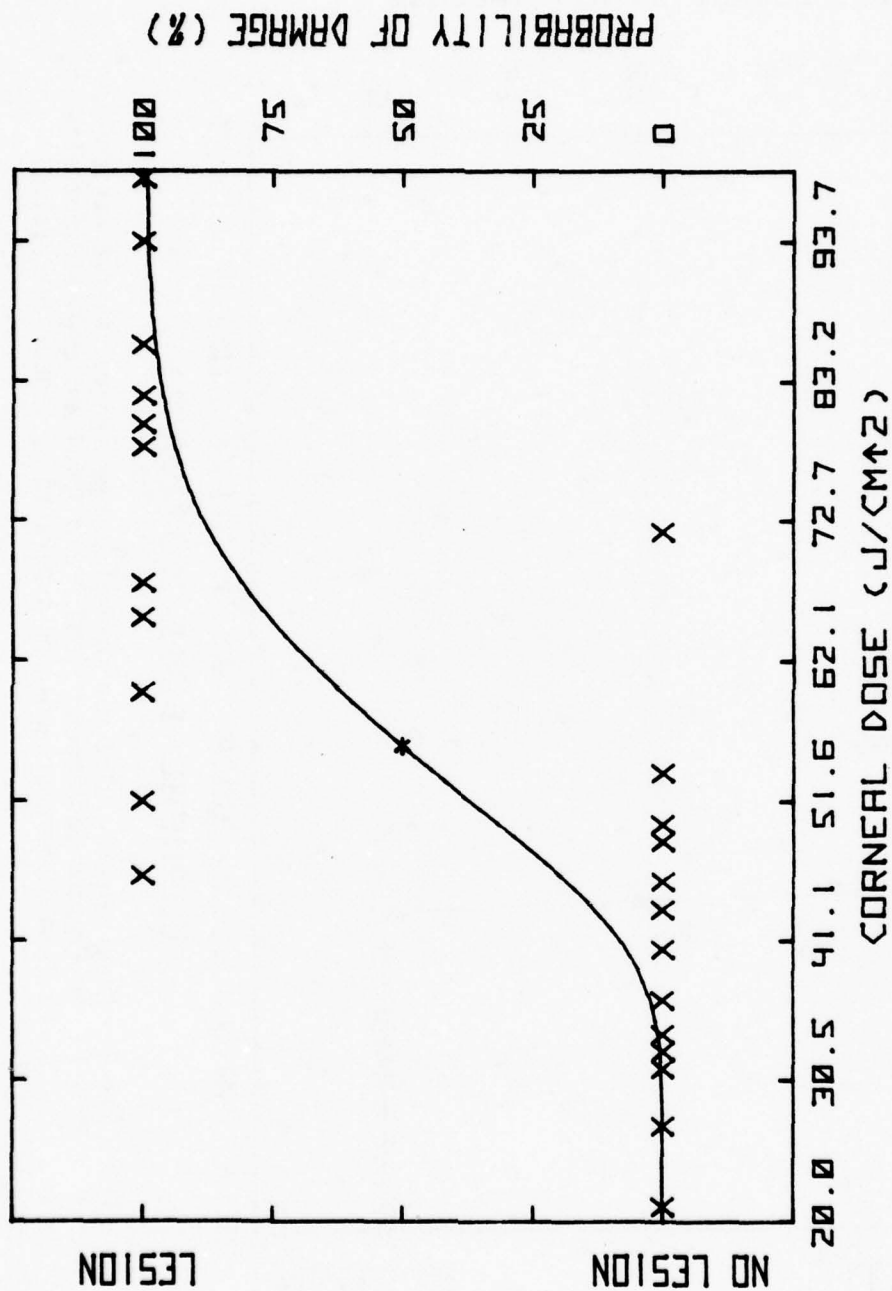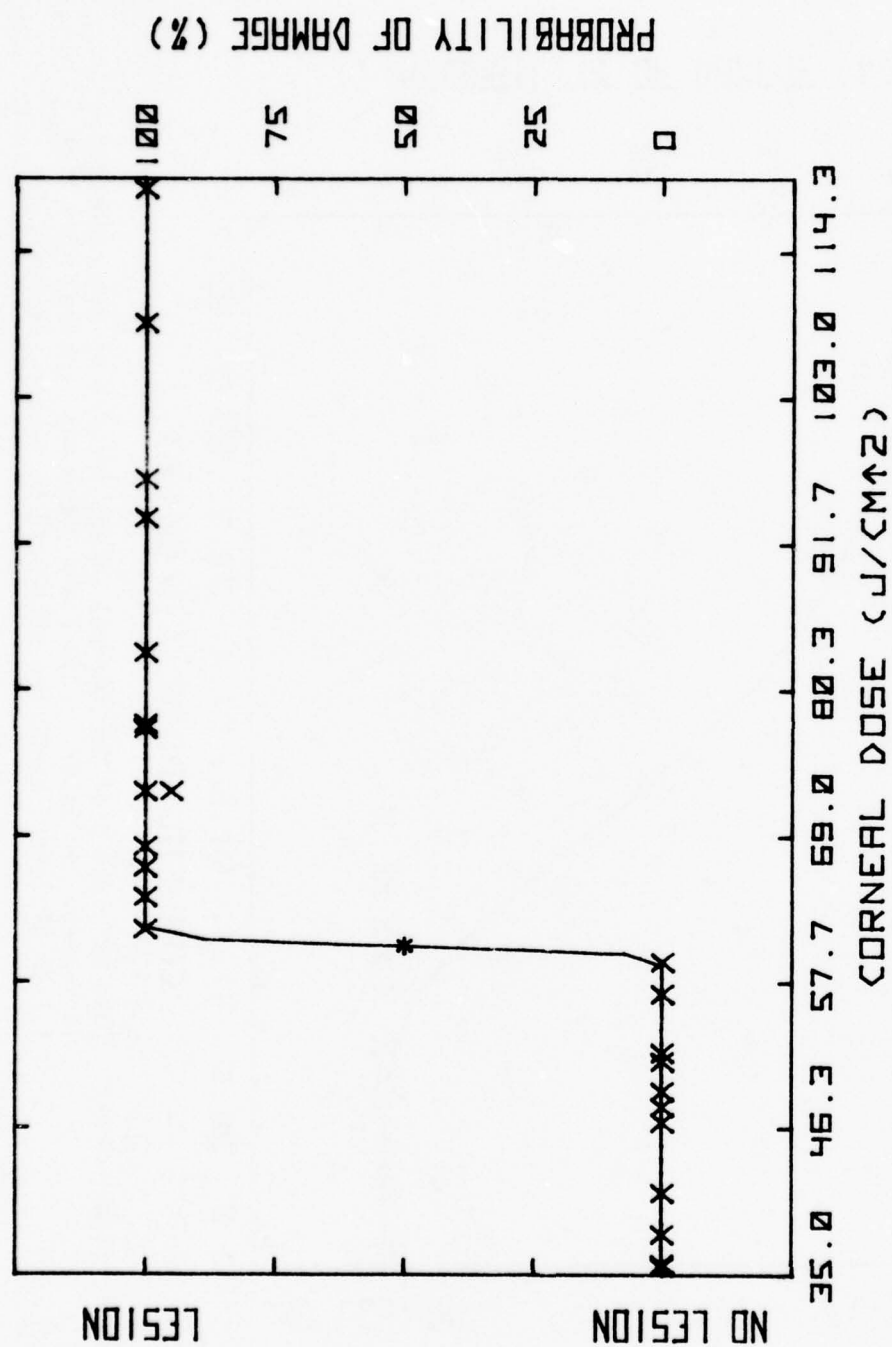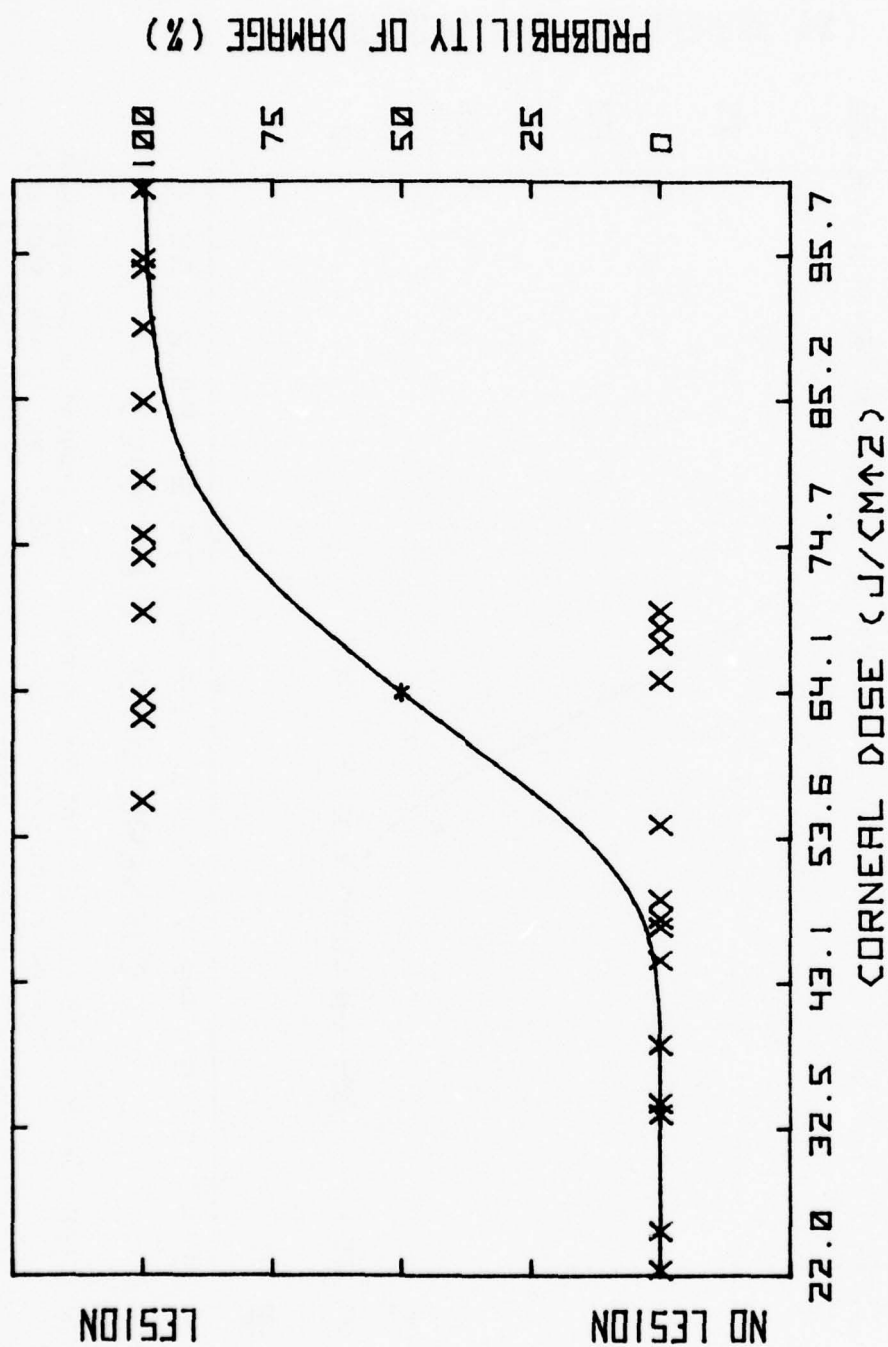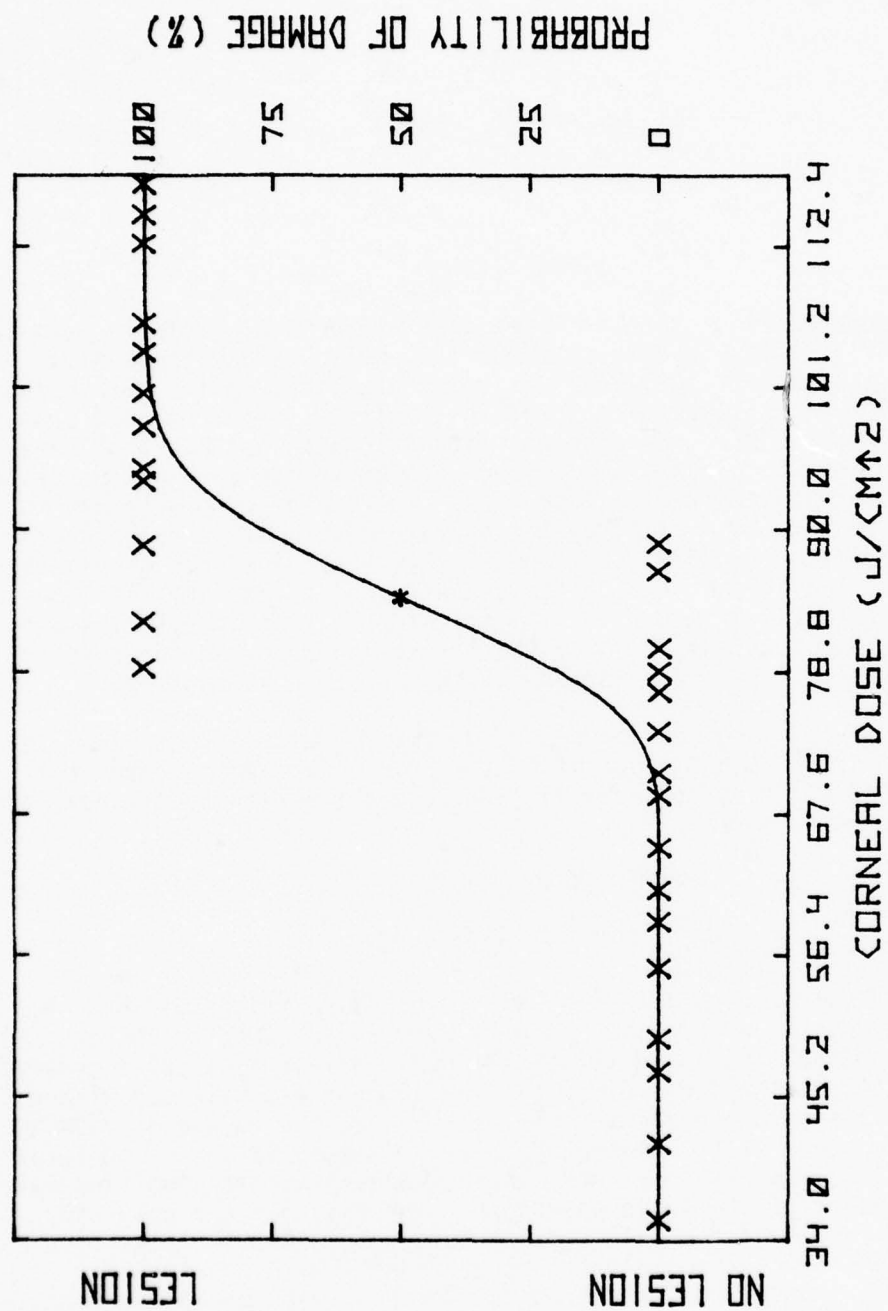
Figure I-A-6. Dose-response plot for corneal damage induced by two exposures to krypton-ion laser. (350.7 and 356.4 nm; corneal spot size 1.7-mm diameter; exposures separated by 48-hour intervals.)

RESEARCH ON THE OCULAR EFFECTS OF LASER RADIATION

PART II

MULTIPLE-PULSE EFFECTS

Gary A. Griess

INTRODUCTION

Because many lasers operate in repetitive-pulse modes, efforts were initiated in the early 1970's to determine multiple-pulse damage thresholds. At the time the ANSI standard Z136.1 (1) was formulated, only a few data points were available for repetitive pulses, and the empirical fit contained proportionate uncertainty. Since then, the experimental data base has considerably expanded, as summarized in Table II-1. The most expansive data was generated by Technology Incorporated (2-5). A prominent feature of this data was an unexpected drop in threshold at a repetition rate near 1 Hz for both argon 514.5-nm and neodymium 1064-nm laser lines. This unusual effect evoked various proposals for mechanisms, and objectives were set to explore this low-frequency multiple-pulse effect. The initial steps were to verify the effect by reproducing the conditions at which the effect was reported to be maximal. The results of this effort are reported in the experimental section.

All attempts to reproduce the reported low-frequency effect have yielded negative results. The significance of this is discussed, and an empirical model is presented which effectively fits the available data by disregarding any special low-frequency anomaly.

EXPERIMENTAL PROCEDURE

Apparatus (Figures II-1 and II-2)

A Spectra-Physics model 170 argon-ion laser operating at 514.5 nm was used at a nominal output of 2 watts. The cw beam was chopped to 10-μsec pulses with an acousto-optical modulator (Datalight DLM1) driven by a pulse generator (General Radio 1340). The first-order diffracted beam was selected with a 3-mm aperture. This gave a maximum power measured at the cornea of 800 mW. To measure the cw power of the diffracted beam, the acousto-optic modulator was driven by a D.C. power supply (H-P Harrison 6289A) with the voltage matched to that of the output of the pulse generator. The external a-o modulator passed cw stray light having a measured intensity about 0.001 times the diffracted beam intensity. This could not be eliminated with apertures so an electro-mechanical shutter was triggered in synchrony with the pulses providing a 10-msec window for the 10-μsec pulse. A Wavetek 164 signal generator was used to generate the trigger pulses at a selected repetition rate. The trigger pulse output was split with a "T" connector, and part of the signal used to trigger a Gerbrands shutter-timer. The other part of the signal was delayed by an adjustable time with a Tektronix 454 oscilloscope. The delayed signal was then used to trigger the General-Radio pulse generator which drove the a-o

TABLE II-1. SUMMARY OF MULTIPLE-PULSE LASER CHORIORETINAL BURN STUDIES

Ref.	Wavelength (nm)	Pulsewidth (sec)	Repetition frequency (Hz)	Pulse-train length (sec)
12	514.5	4.0×10^{-5}	CW, 100, 1000	0.1, 0.5, 1.0
2	514.5	1.0×10^{-5}	2, 10, 100, 10^3, 10^4	0.5
5	514.5	10^{-3}	10, 10^2	0.5
		10^{-3}	1, 10, 10^2	5.0
		10^{-4}	10, 10^2, 10^3	0.5
		10^{-5}	40, 10^2, 10^4	0.05
		10^{-5}	2, 4, 10, 10^2, 10^3	0.5
		10^{-5}	0.4, 0.6, 1, 10, 10^4	5.0
		10^{-5}	0.1, 0.2, 0.4, 1, 10, 10^4	30.0
		10^{-5}	0.1, 0.17, 0.25, 0.6, 1.0	$2/R$ [a]
		2×10^{-6}	0.5, 0.0333	$2/R$ [a]
7	532	1.5×10^{-8}	5	30, 120
16	694.3	2×10^{-4}	1.67×10^{-2}, 5.55×10^{-3}	7-17 pulses
8	858	5×10^{-7}	1.2×10^5	0.125, 0.5, 1.0, 8.0
9	905	3.0×10^{-8}	40, 1000	22, 0.72 [b]
4	1064	3×10^{-7}	40, 10^2, 10^4	0.05
			4, 10, 10^2, 10^3, 10^4	0.5
			1, 10, 10^2, 10^3, 10^4	5.0
			0.1, 0.2, 1, 10, 10^2	103, 30
11	1064	1×10^{-8}	10, 20	0.5, 1.0
10	1064	1.8×10^{-8}	10^3	(1,2,5,74) $\times 10^{-3}$, 1.0
		1.8×10^{-8}	10^2	0.01, 0.02

[a] R = Repetition frequency

[b] ED_{50} exposure time
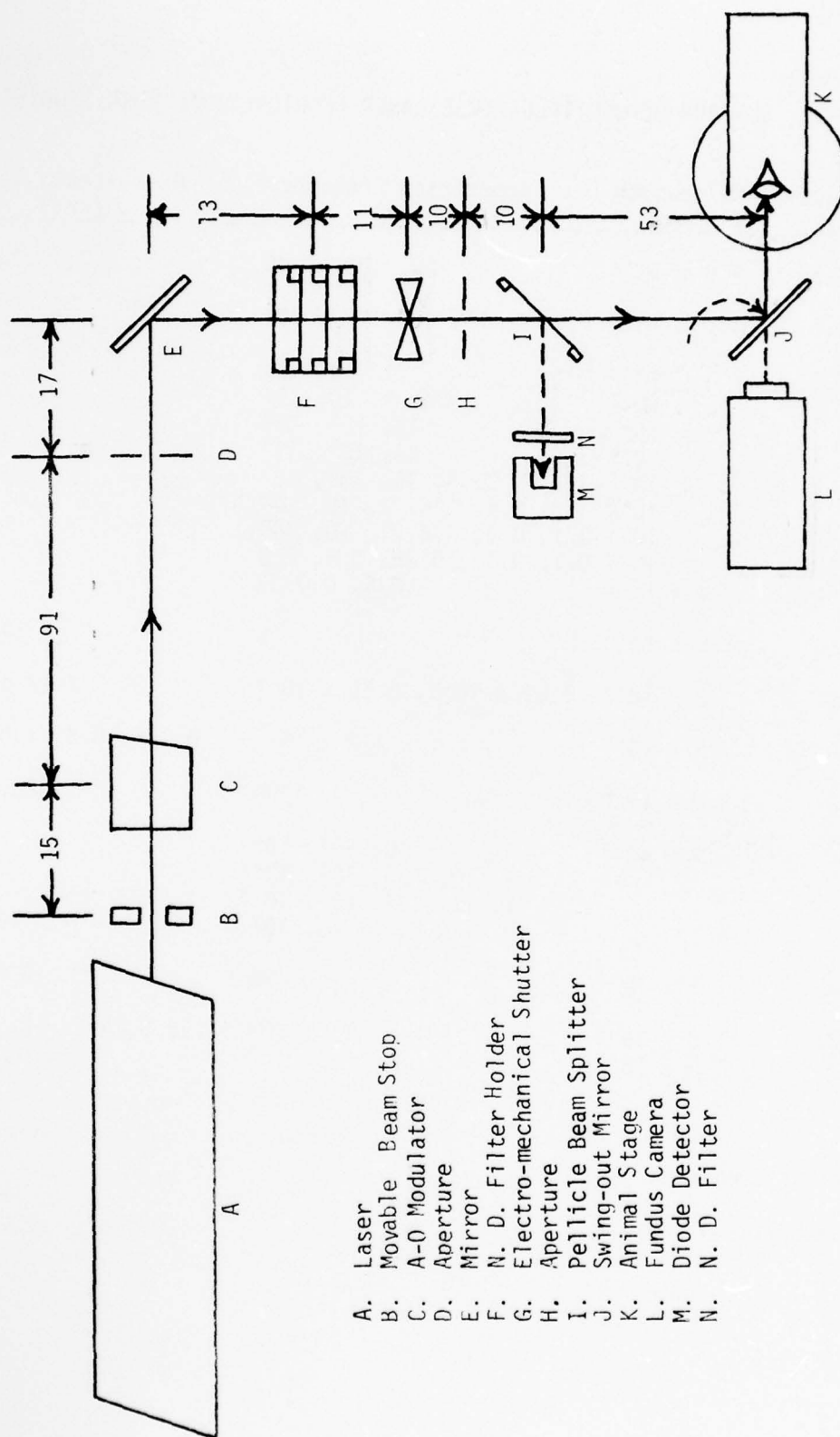
A. Laser
B. Movable Beam Stop
C. A-O Modulator
D. Aperture
E. Mirror
F. N. D. Filter Holder
G. Electro-mechanical Shutter
H. Aperture
I. Pellicle Beam Splitter
J. Swing-out Mirror
K. Animal Stage
L. Fundus Camera
M. Diode Detector
N. N. D. Filter

Figure II-1. Optical system. (Dimensions in cm; not drawn to scale.)
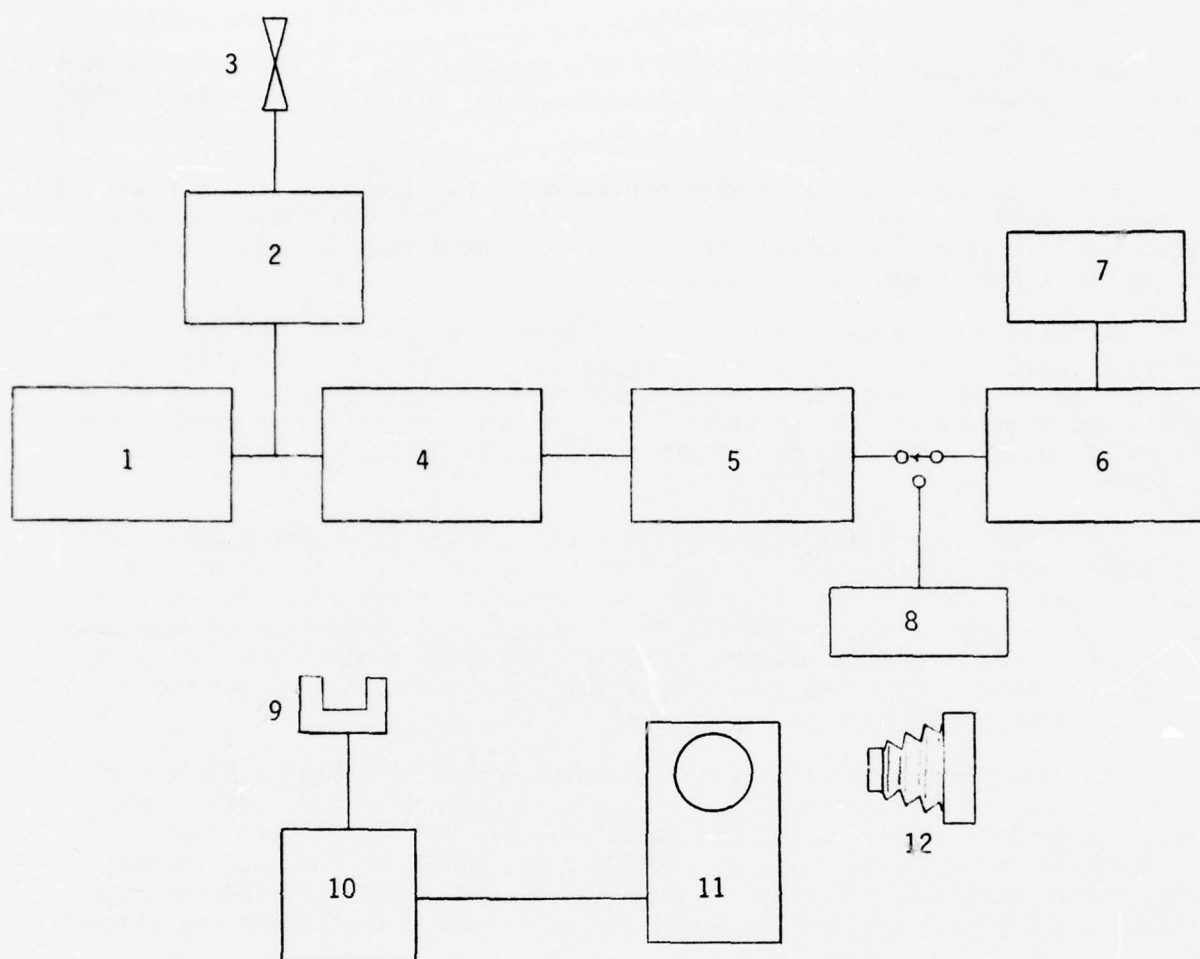
1. Frequency Generator
2. Shutter Timer
3. Shutter
4. 454 Oscilloscope Delay Trigger
5. Pulse Generator
6. Acousto-optic Control

7. A-O Modulator
8. DC Voltage Supply
9. Diode Detector
10. Bias Supply
11. 555 Oscilloscope
12. Camera

Figure II-2. Electronic system.

modulator with square 10-μsec pulses. This centered the 10-μsec pulse in the 10-msec window to assure that no pulses were being cut by the relatively slow response of the mechanical shutter.

Beam power was attenuated with neutral-density filters. It was found that a thermal lensing effect occurred in the filters. This was circumvented by stacking filters having optical densities no greater than 0.3 and, also, by using short pulses at low duty cycle.

The beam profile was measured with a photodiode (shielded by a 50-μm pinhole) mounted on a motor-driven micrometer stage. The amplified output of the photodiode was recorded with a Hewlett-Packard X-Y recorder. The beam width was measured at $1/e^2$ points. Divergence was determined by taking beam scans at several positions on the optic axis. The measured divergence was 0.7 mrad.

A pellicle beam splitter deflected a part of the beam onto a EG&G SGD444 photodiode detector with a 90-V bias supply. A 0.9 OD filter and diffuser were placed in front of the diode to guard against saturation. The detector output was monitored on a Tektronix oscilloscope. For experimental exposures a record of the amplitude of each pulse was made with photographs of the oscilloscope trace. It is estimated that the pulse amplitudes as determined from the photographs were accurate to within 3%.

The diode detector output was calibrated before and after experimental exposure sessions. Power at the cornea was measured with a Scientech 3600 laser power meter for each combination of neutral-density filters used. A calibration curve of corneal power versus pulse height on the oscilloscope was generated (Fig. II-3). The calibration of the filters provided an additional means of calculating the pulse energy in case a photograph was unusable.

The power meter calibration was traceable to the National Bureau of Standards. The measurement of energy of an individual 10-μsec pulse posed a problem. The energy of a train of pulses could be measured with a TRG-100 ballistic thermopile coupled to a Keithley microvoltmeter. A consistent value for the energy per pulse for a variety of train lengths and repetition rates affirmed the validity of this calibration method.

A third calibration procedure used a calorimeter and nanovoltmeter. The energy of 10-μsec pulses could be measured reproducibly to within 10%. However, the "window" of the background light made a large (70%) contribution which had to be subtracted. This latter procedure gave values of energy per pulse about 15% lower than those calculated from the first procedure (Scientech power meter). On the other hand, the TRG-100 thermopile procedure gave values about 15% higher than the Scientech measure. Each of the three procedures has its own merits and deficiencies, so that one cannot be considered more reliable than the others. Although the procedure using the Scientech meter is the least direct, it gave values midway between the other two methods, which makes it nearest to the most probable reading. This procedure is also the most convenient for routinely calibrating the diode detector over the whole range of filter factors, so it was the one adopted as the primary method.

A Zeiss fundus camera was mounted with its axis orthogonal to the laser beam. A swing-out mirror mounted on the objective of the fundus camera allowed the beam to be aligned with the camera axis for precise location of exposure sites.
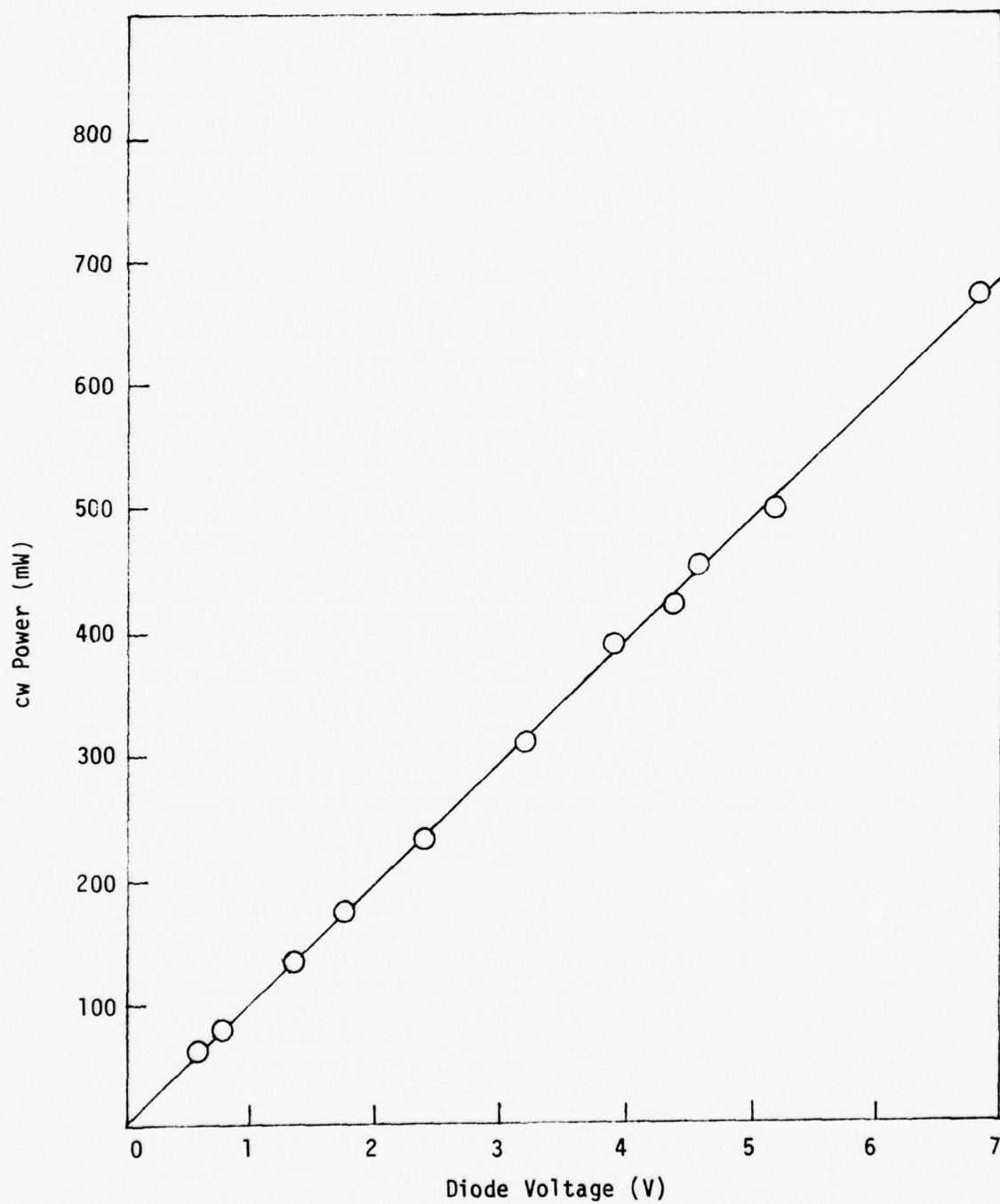
Figure II-3. Calibration curve of power at cornea vs. diode output.

Animal Exposures

Owing to unavailability of rhesus monkeys (<u>Macaca</u> <u>mulatta</u>), <u>Macaca</u>
<u>fascicularis</u> were used for most of this work. Prior to exposure, cycloplegia
was induced by administration of atropine sulfate. Subjects were tranquilized
with an intramuscular injection of ketamine hydrochloride (10 mg/kg) and anes-
thetized with sodium pentobarbital introduced into a posterior superficial
vein in one leg. Initially, 0.5 ml of sodium pentobarbital (50 mg/ml) was
injected with 0.1-ml increments introduced as necessary to maintain the de-
sired degree of anesthesia. To reduce eye movement, retrobulbar injections
of 2% lidocaine were administered (0.4 ml temporal, 0.2 ml nasal).

During laser exposures and retinal examination the eyelids were held
open by means of a wire speculum. To preserve corneal transparency the eye
was irrigated frequently with normal saline from an electrically controlled
atomizer. Two orthogonal rows of marker burns were placed in the paramacular
region to provide 4 x 4 grid coordinates. Sixteen exposures were presented
at these sites in incremental steps of peak power varied by neutral-density
filters. The eyes were examined funduscopically at 1 hour and 24 hours post
irradiation and judged for minimum visible lesions.

Two animals were sacrificed for histopathologic evaluation. In these
cases only nine ocular sites were exposed in a 3 x 3 array. Single-pulse and
multiple-pulse exposures were alternately placed in each eye at near thresh-
old levels. One eye was exposed approximately 24 hours after the other and
just before sacrifice so that the development of lesions could be seen at $\sim$1
hour and 24 hours post exposure. Immediately after the final exposure,
fluorescein angiography was performed on the animal with the intention of
obtaining a map of the eye to assist in histological sectioning.

To adjust for variability in threshold between animals, experiments were
designed so that thresholds obtained for a pair of eyes from each animal could
be compared. Thus a multiple-pulse threshold determined for one eye could be
normalized with the single-pulse threshold determined for the other eye of
the same animal.

Initially, a train of five 10-μsec pulses at a repetition rate of 1 Hz
was chosen for direct comparison with the earlier reported work, as this was
the condition where the effect was maximal. When it appeared that the effect
was not being reproduced, different repetition rates were tried, while keeping
the number of pulses fixed at five. In this latter case, each eye of a given
animal was exposed at a different pulse-repetition rate so that a relative
threshold could still be determined without determining additional single-
pulse thresholds.

Two independent observers evaluated the eyes for minimal lesions. Both
observers examined the retinas at the time of exposure to minimize confusion
due to artifacts such as drusen. Judgment was on a basis of "burn" or "no
burn." Disagreement between the two observers or uncertain judgments were
cast out of the combined evaluations used in the data analysis. The 50% pro-
bability of damage level was calculated by probit analysis on a H-P 9830A
computer. Thresholds for both 1 hour and 24 hours post exposure were deter-
mined for each of the five exposure conditions: single-pulse and five-pulse
trains at 0.25, 0.5, 1, and 2 Hz.

RESULTS

Thresholds from fourteen pairs of eyes are reported in Tables II-2 and II-3. Cases where there was any question of the validity of the data, such as when equipment malfunctioned, were excluded. From four to seven eyes were exposed for each pulse configuration. This number proved to be sufficient for the determination of thresholds with acceptable confidence levels. The average values and standard deviations calculated from the single-eye ED_{50}'s for each pulse configuration are shown at the bottom of each table. Also included are the combined probits (with 95% confidence limits) obtained by a single probit calculation using all of the data from the four to seven eyes for each pulse configuration.

The primary objective was to compare the single-pulse threshold with the multiple-pulse 1-Hz threshold. It had been reported earlier that for a five-pulse train at 1 Hz, there was a factor of six decrement in the multiple-pulse threshold relative to the single-pulse threshold. However, in this work, the decrement was at most a factor of two. In anticipation that the decrement was critically dependent on pulse-repetition rate, other frequencies (0.25, 0.5, 2 Hz) were examined. The threshold for these frequencies was not substantially different from that for 1 Hz.

Several observations can be made about the data. First, there is a discernible lowering of threshold for 24 hours post exposure (Table II-3) as compared to 1 hour post exposure (Table II-2). This has been observed by others and may be attributed to a combination of temporal development of lesions and recovery of corneal clarity.

Another observation concerns the different ways of looking at the thresholds. One way was to compare thresholds from the two eyes of a given subject. Thus, for example, the ratio of the single-pulse threshold from one eye to the multiple-pulse threshold energy per pulse from the second eye should give a normalized measure of the change in threshold. This ratio varied from 1.0 to 2.3 with a mean of 1.7. The other way of treating the data was to compile evaluations for all of the eyes for each set of conditions. This procedure smooths out the variations and gives a sharper definition of threshold. The composite multiple-pulse thresholds may also be normalized relative to the composite single-pulse threshold. The ratios are 1.92 and 1.79 for 1 Hz at 1 hr and 24 hrs, respectively.

It had been assumed that variations in threshold are due primarily to individual differences such as degree of pigmentation, refractive error, or metabolism. Since these factors are usually more closely matched for the two eyes of any given subject than for eyes from different subjects, this assumption would predict a strong correlation of thresholds for pairs of eyes of each subject. This is not supported by the evidence. The deviations in threshold between pairs of eyes (as indicated by ratios) are as great or greater than the deviations from the norm.

When it was found that the factor of six reduction in the multiple-pulse threshold could not be reproduced, it was decided to repeat the experiment with newly acquired rhesus monkeys in order to test the possibility of a species specific effect. Two rhesus monkeys received single-pulse exposures in

43

TABLE II-2. ED$_{50}$ THRESHOLDS FOR 1-HOUR POSTEXPOSURE EVALUATIONS
(514.5-nm, 10-μsec pulses. Single-pulse and 5-pulse trains.)

| Primate No. | ED$_{50}$ (mW/pulse) | | | | | ED$_{50}$(eye 1)/ ED$_{50}$(eye 2) |
| | Single pulse | Pulse-repetition rate (Hz) | | | | |
		0.25	0.5	1.0	2.0	
27	270			244		1.14
29	418			192		2.30
39	208			208		1.00
47	481			(397)[a]		1.21
49	512			234		2.19
82	229	189				1.21
89	504	222				2.27
83		134			131	1.02
85		261			146	1.79
75		163	205			0.80
73			105		150	0.70
69			162		190	0.85
57			141	132		1.07
41				175	214	0.82
Average	376±124	194±44	153±36	195±38	166±31	
Combined Probit	280±35	208±4	138±17	146±27	177±27 mW/pulse	
	7.3±0.9	5.4±0.1	3.55±0.4	3.8±0.7	4.6±0.7 μJ/cm^2/pulse	

[a] Anomalous value, not included in average or combined probit.

TABLE II-3. ED$_{50}$ THRESHOLDS FOR 24-HOUR POSTEXPOSURE EVALUATIONS
(514.5-nm, 10-μsec pulses. Single-pulse and 5-pulse trains.)

| Primate No. | ED$_{50}$ (mW pulse) | | | | | ED$_{50}$(eye 1)/ ED$_{50}$(eye 2) |
| | Single pulse | Pulse-repetition rate (Hz) | | | | |
		0.25	0.5	1.0	2.0	
27	228			222		1.03
29	285			176		1.62
39	177			95		1.36
47	412			195		2.11
49	346			234		1.48
82	229	137				1.67
89	318	147				2.16
83		(40)[a]			b	-
85		147			127	1.16
75		128	121			1.06
73			105		182	0.58
69			140		136	0.75
57			141	145		0.97
41				155	162	0.96
Average	285±75	140±8	127±15	175±44	164±23	
Combined Probit	242±27	127±4	138±7	135±4	165±4 mW/pulse	
	6.3±0.7	3.3±0.1	3.6±0.2	3.5±0.1	4.3±0.1 μJ/cm^2/pulse	

[a] Anomalous value, not included in average or combined probit.

b 24-hour threshold not obtained due to clouding of ocular media.

one eye and 1-Hz five-pulse trains in the other. The multiple-pulse threshold for both 1 hour and 24 hour postexposure evaluations was 3.4 ± 0.2 µJ/cm²/pulse. This compares with 3.8 ± 0.7 and 3.5 ± 0.1 µJ/cm²/pulse for _Macaca fascicularis_ thresholds at 1 and 24 hours, respectively. The single-pulse rhesus threshold was 6.8 ± 1.5 µJ/cm²/pulse at 1 hour post exposure compared with 7.3 ± 0.9 for _Macaca fascicularis_. At 24 hours post exposure, the threshold for one of the animals changed very little from the 1-hour evaluation in agreement with the results for _Macaca fascicularis_. In the second animal, all sixteen single-pulse exposure sites developed visible lesions at 24 hours. A similar 24-hour post exposure development occurred in one _M. fascicularis_ eye (#830D) exposed to a 0.25-Hz pulse train. The inclusion of these data points in a relatively small sample population would displace the threshold towards a much lower value. We can offer no explanation for these anomalies except to note that the thresholds for these eyes were typical at 1-hour post exposure. It therefore seems unlikely that the low frequency effect reported by Connolly et al. (5) was due to the same phenomenon.

Histopathology of multiple-pulse retinal lesions was called for because it was believed it could help identify the mechanism of the multiple-pulse effect which this work sought to verify. The absence of the pronounced threshold decrement reduced the concern for mechanism, and the importance of histological studies is, thereby, diminished. The eyes from only one of the animals sacrificed were usable, and the report on that is still forthcoming. A preliminary light microscopic viewing of the sections indicated that the gross appearance of multiple-pulse lesions is the same as single-pulse lesions. Damage appears mainly in the retinal pigment epithelium, and it is typical of thermal lesions. The full report on the histopathology will appear at a later date.

DISCUSSION

The first objective of this work was to verify the low-frequency multiple-pulse effect reported earlier (5). While a decrement in threshold was found, the magnitude was much less than the earlier reported effect. Even if the reported low-frequency effect was not an artifact, its magnitude is such that it lies within the scatter of the multiple-pulse data base, and in formulating a safety standard no specific provision need be made for this effect. It is therefore possible to formulate a general empirical model for multiple-pulse thresholds as discussed in the following paragraphs.

The parameters of wavelength, λ, pulsewidth, t, pulse-repetition rate, R, and train length, T, form a multidimensional space for retinal thresholds. If the threshold is expressed as total intraocular energy (TIE = N x ED_{50}) for a train of N pulses, and total-on-time is defined as TOT = RTt = Nt, an empirical relationship may be found from the log-log plot of TIE vs. TOT for the experimental data base. For each pulsewidth the locus of points is one of a family of lines which are approximately parallel to the rising portion of the single-pulse (cw) threshold curve. This part of the curve is described by:

$$ED_{50}(J) = At^{3/4}$$

where t is the exposure duration and A incorporates the wavelength dependence. The cw threshold curve has two constant-energy plateau regions: below the breakpoint t_b = 18 µsec and above the breakpoint t = 10 sec (for visible wavelengths).

The relationship of multiple-pulse and single-pulse thresholds is shown schematically in Figure II-4. If the repetitive pulses have a pulsewidth greater than the lower breakpoint t_b, the locus of multiple-pulse thresholds will coincide with the cw threshold curve. That is:

$$TIE = A(TOT)^{3/4}$$

If the pulsewidth is less than t_b, however, the limit of N = 1 means that the locus of multiple-pulse thresholds intersects the cw constant-energy plateau at the exposure duration of the pulsewidth, t. As seen in the diagram, this translates the multiple-pulse threshold curve away from the parallel single-pulse threshold curve by an amount:

$$\Delta \log t = \log t_b - \log t = \log (t_b/t)$$

For this case of $t < t_b$ the multiple-pulse threshold TIE may be related to the cw threshold by:

$$\log TIE = \log A + 3/4 \{\log (RTt) + \log (t_b/t)\}$$

or:

$$\log TIE = \log A + 3/4\{\log (RTt_b)\}.$$

If we define an adjusted total-on-time TOT' = RTt_b, then:

$$TIE = A(TOT')^{3/4}.$$

This is summarized in the following procedure:

(1)   For pulsewidths $t > t_b$, the total-on-time is defined as:
$$TOT = RTt.$$

The threshold total intraocular energy is related to the cw threshold at duration equal to TOT by:

$$TIE = A(TOT)^{3/4}$$

(2)   For pulsewidths $t < t_b$, the adjusted total-on-time is defined as:

$$TOT' = RTt_b.$$

The threshold total intraocular energy is related to the cw threshold at duration equal to TOT' by:
$$TIE = A(TOT')^{3/4}$$

The threshold energy per pulse is TIE/N, and the maximum permissible exposure (MPE) is related to threshold by a safety factor of 10.

The cw threshold limits put constraints on the range of applicability of the TOT model. The wavelength range is $400 \leq \lambda \leq 1400$ nm, and the pulsewidth range is $10^{-9} \leq t < 10^4$ sec. The upper constant-energy plateau region (durations greater than 10 sec) places additional constraints. That is, it is questionable to extrapolate beyond a total-on-time of 10 seconds. This sets a combined limit to pulsewidth, repetition rate, and trainlength: TRt $\leq$ 10 sec.
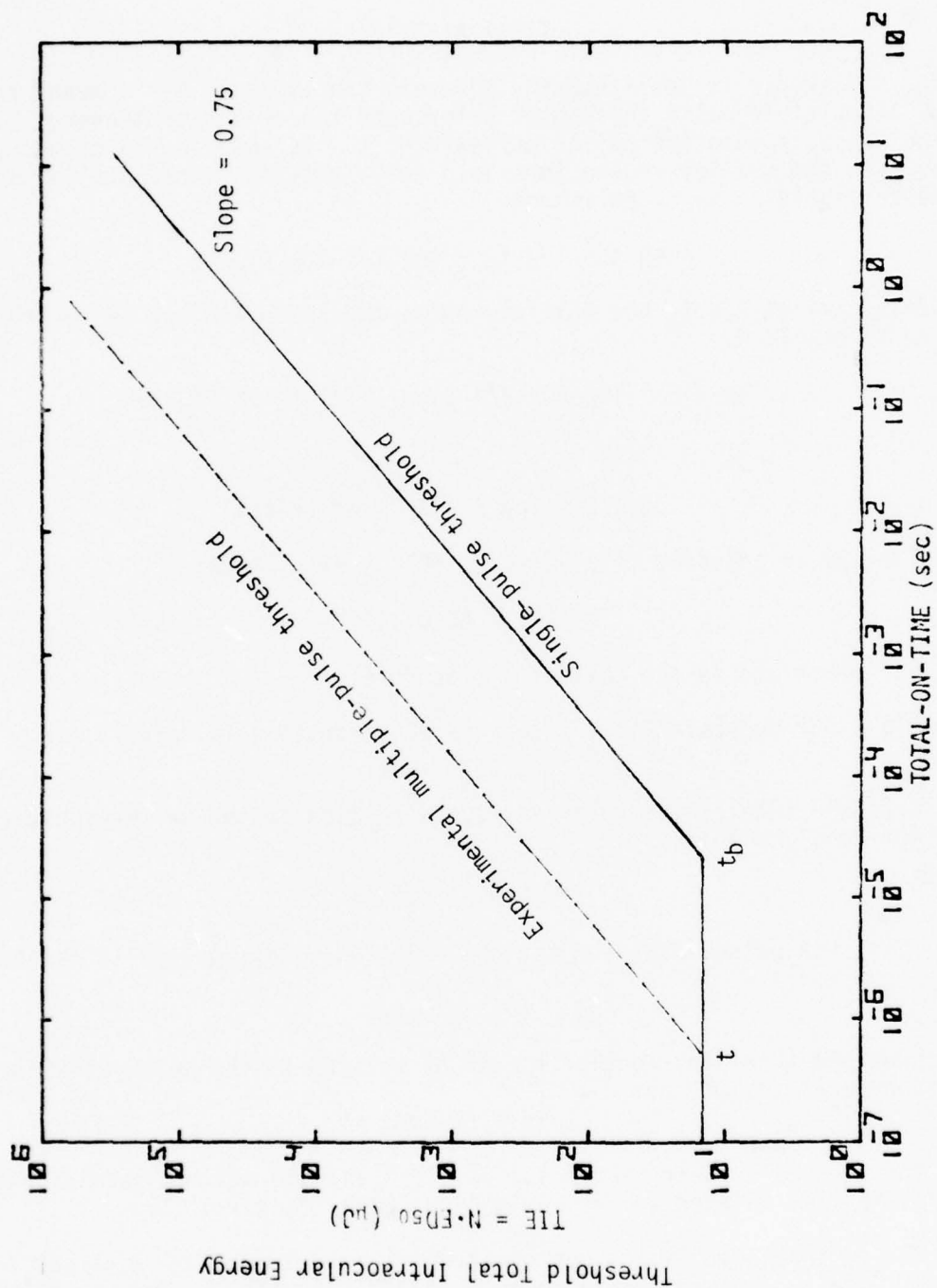
47

Figure II-4. Relation between multiple-pulse and single-pulse thresholds. TOT = RTt = Nt.

Taking note of the fact that the duty cycle, Rt, is always less than unity, the primary constraint is for the trainlength:

$$T \leq \frac{10}{Rt} .$$

It is doubtful that direct intrabeam viewing of a repetitively pulsed laser beam would reach this duration in practice.

The current ANSI standard uses the TOT basis for pulses greater than t_b, but a less satisfactory procedure is used for pulses shorter than t_b. There the single-pulse MPE is decreased by a reduction factor (Figure II-5) which is a variable function of repetition rate only. It is therefore difficult to compare the two methods on an equal basis.

The current ANSI standard for multiple-pulse exposures was empirically fitted to the then-available data (solid symbols in Figure II-5). When subsequent data points (open symbols) are plotted on this same figure, the deficiencies become apparent. First, the reduction factor was based only on repetition rate, while trainlength was neglected. Second, additive effects were assumed not to extend to repetition rates below 1 Hz. While the evidence contradicts this assumption, no data tell at what pulse-separation the repair rates cancel cumulative, subthreshold damage effects. At this time, it seems best to leave open the lower limit of pulse-repetition rate. The same data points shown in Figure II-5 are plotted in Figure II-6 according to the total-on-time basis outlined here. There appears to be a good fit over the whole range of parameters. The TOT approach has been further tested with other multiple-pulse thresholds from the literature (7-11), which for the most part confirm the model. The greatest disagreement between experiment and model is the data of Ebbers and Dunsky (11) for trains of 10 nsec, 1064-nm pulses. It should be noted that their thresholds were for paramacular lesions, and their single-pulse threshold is proportionately high.

In Figure II-7 and II-8 an attempt is made to compare the two models on a TIE vs. TOT plot. There are two cases where the ANSI model shows maximal difference from the TOT model: $R \leq 1$ Hz and $R \geq 250$ Hz. In the first case (Fig. II-7), the ANSI model predicts higher thresholds than the TOT model, and the difference is greatest at high total-on-time (long trains). In the second case (Fig. II-8), the ANSI model predicts lower thresholds with maximum difference at low total-on-time (short trains). In both cases, the maximum difference is over an order of magnitude. The experimental data points tend to occur where the differences between the models are smallest, so a judgment is not as decisive as would be desired. However, the TOT model is favored by the fit of the data. Along with this, the consistency and simplicity of the TOT model recommend it as a replacement of the current ANSI standard for repetitive pulses. It should be realized that this, too, is an empirical model which could be superseded by a successful mechanistic model.

The empirical model proposed by Stuck et al.(13) (Army model) has similarities to the TOT model which can be seen by writing their expression for total intraocular energy:

$$TIE = 3.5 \; ARtT^{3/4} \quad \text{for } t > t_b$$

and

$$TIE = 3.5 \; ARt_bT^{3/4} \quad \text{for } t < t_b.$$

49

PULSE-REPETITION RATE (Hz)

REDUCTION FACTOR (% of single-pulse MPE)

△ 1064 nm, 280 nsec, Hemstreet et al. (4)
○ 514.5 nm, 10 μsec, Connolly et al. (5)
▽ 514.5 nm, 10 μsec, Griess (6)
● 514.5 nm, 10 μsec, Skeen et al. (2)
▲ 1064 nm, 280 nsec, Skeen et al. (3)
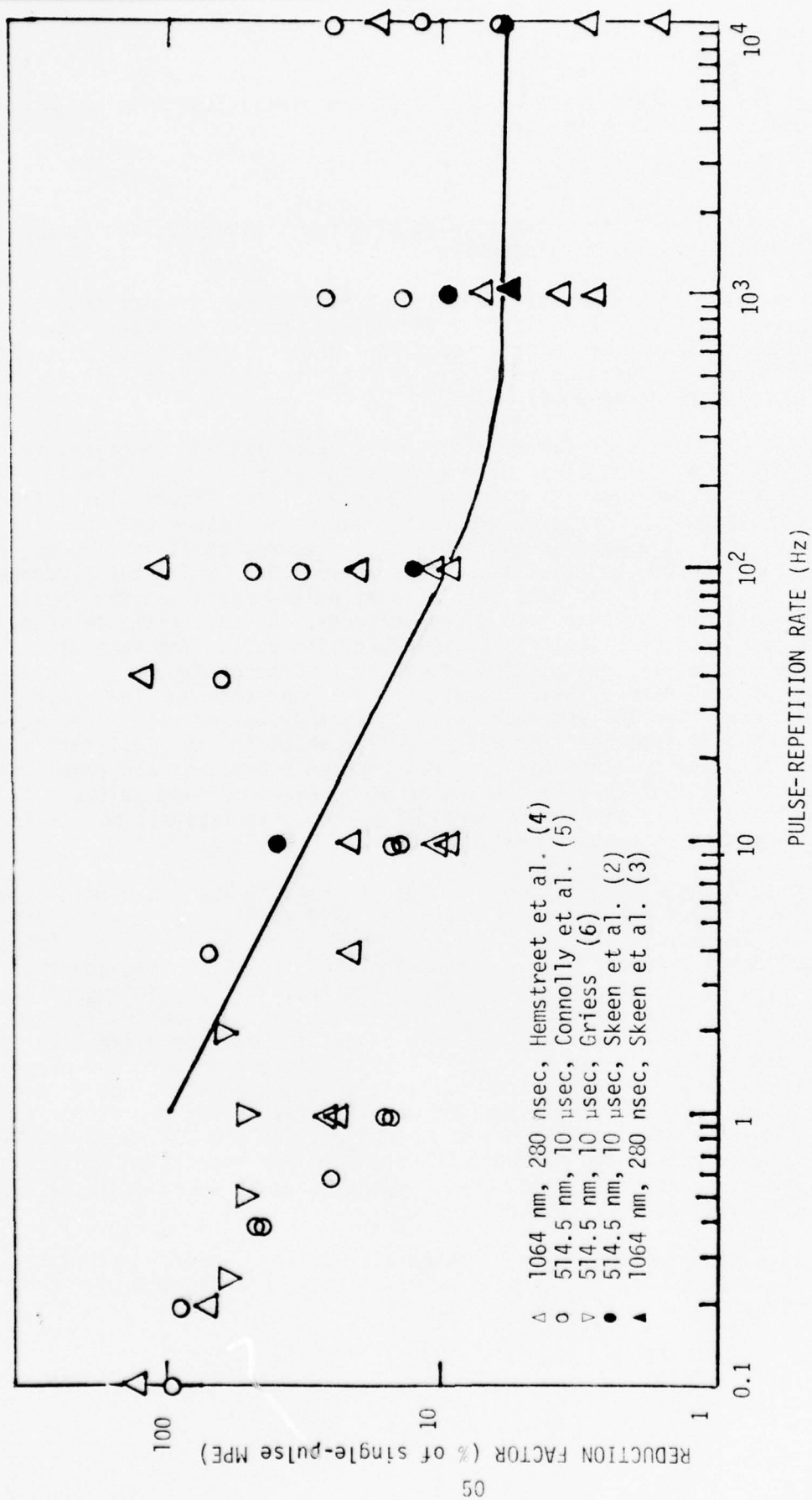
Figure II-5.   Multiple-pulse reduction factor as function of pulse-repetition rate.
Solid line is function in ANSI Z136.1 fitted to solid data points from
References 2 and 3.

50
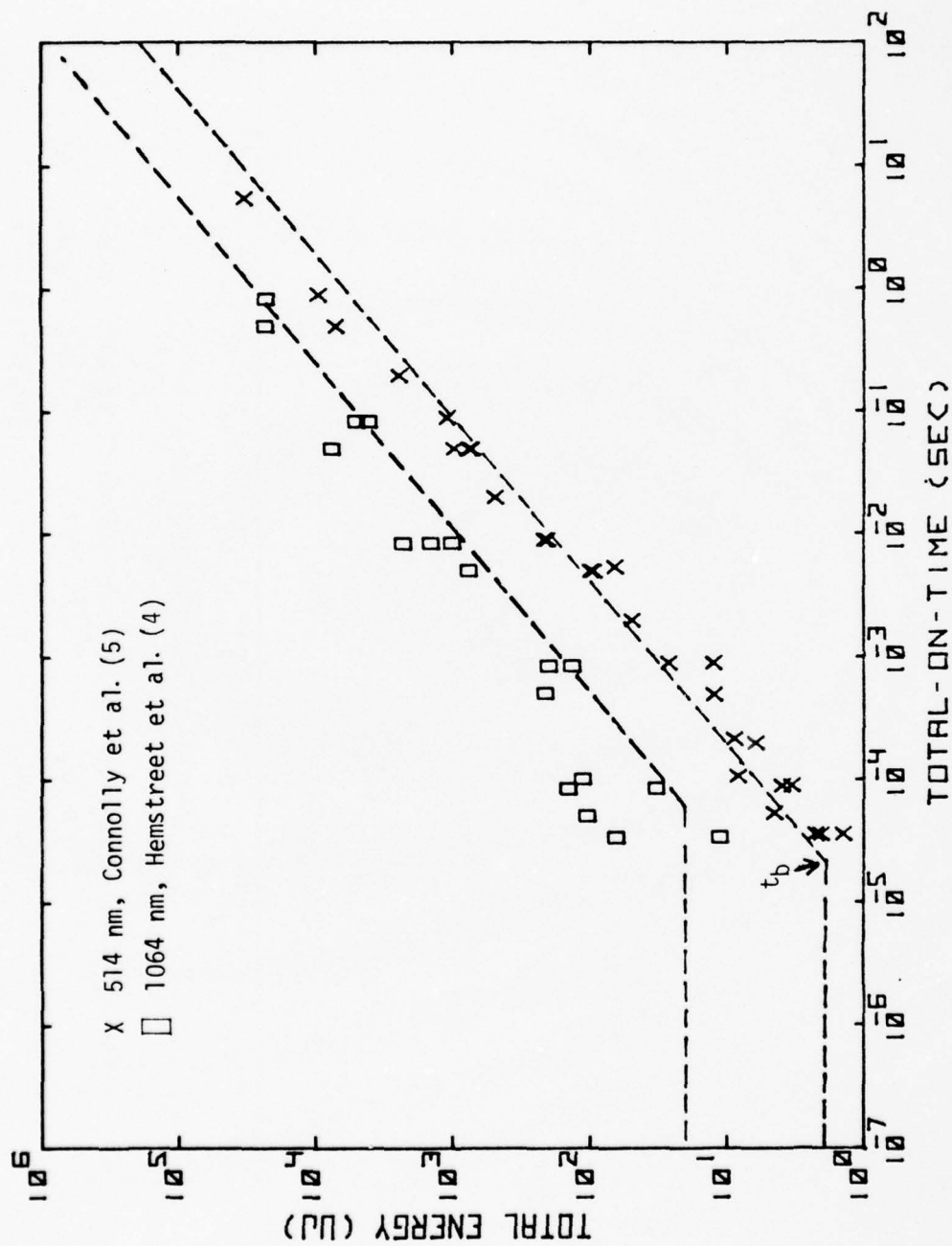
Figure II-6. TIE vs. adjusted TOT (RTt_b).
Broken lines are cw thresholds.

ADJUSTED TOTAL-ON-TIME (sec)

TOTAL ENERGY (uJ)
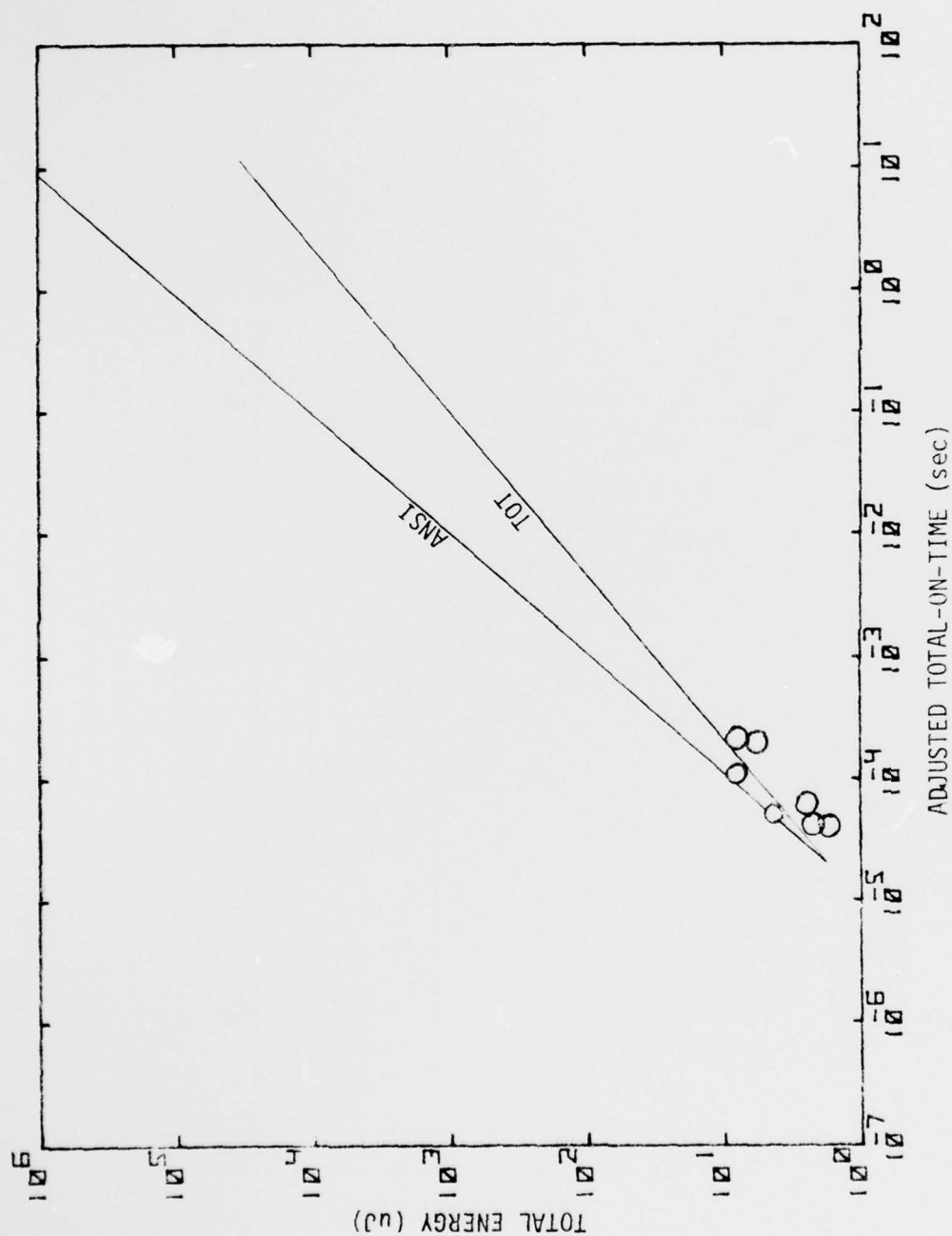
Figure II-7. Comparison of ANSI and TOT multiple-pulse models.
$R \leq 1$ Hz, $\frac{1}{R} < T \leq \frac{10}{Rtb}$, 514.5-nm, 2- and 10-μsec pulses.
o - Experimental points from Connolly et al. (5)

ADJUSTED TOTAL-ON-TIME (sec)
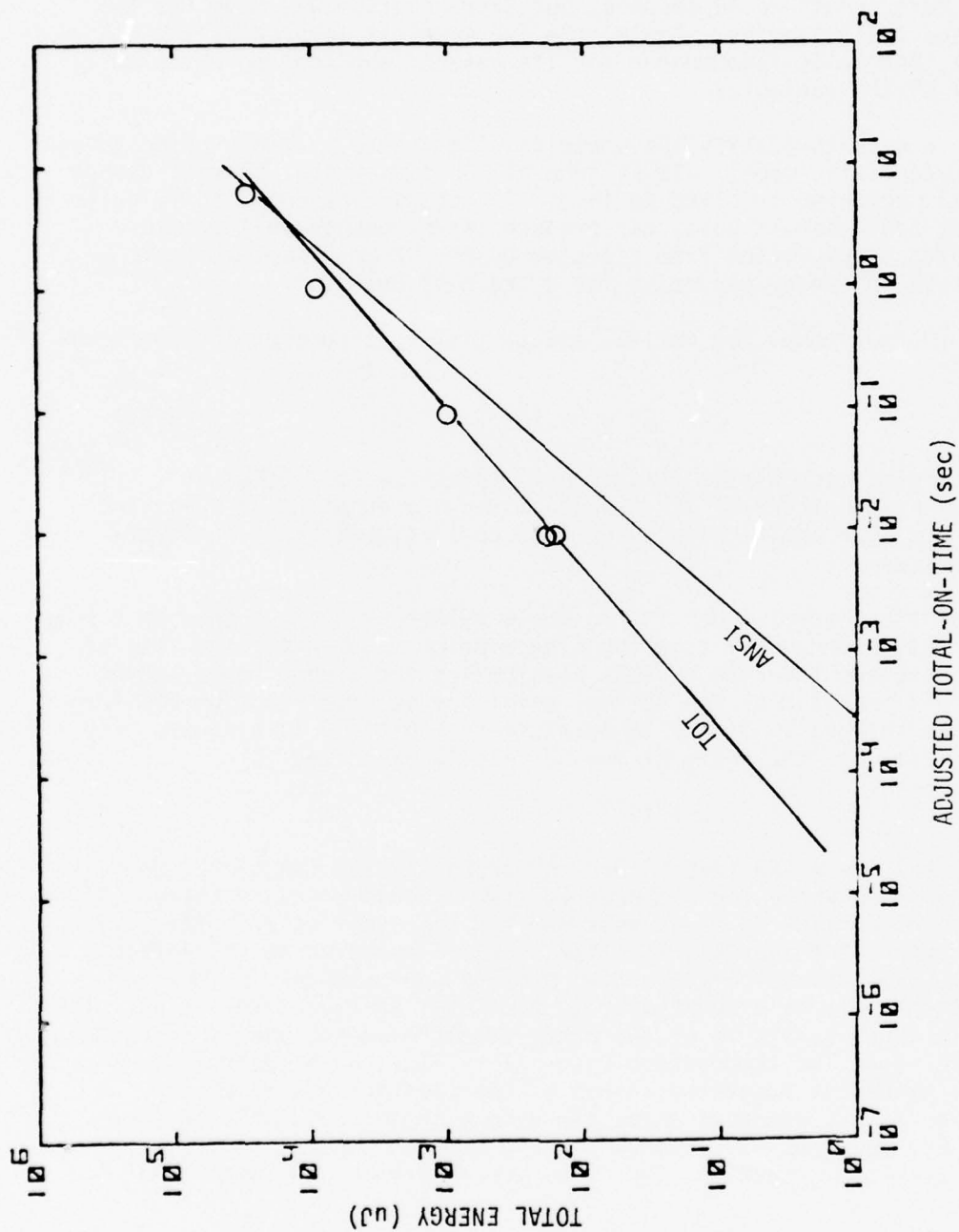
Figure II-8. Comparison of ANSI and TOT multiple-pulse models.

$R \geq 250$ Hz, $\frac{1}{R} < T \leq \frac{10}{Rt_b}$, 514.5-nm, 10-$\mu$sec pulses.

o - Experimental points from Connolly et al. (5)

This is seen to differ from the TOT model by the correction factor of 3.5, as well as in the exponents of R and t. If these two models are compared on the TIE vs. TOT plot, the Army model gives a family of parallel lines for different fixed values of train length while repetition rate is varied from single-pulse to continuous duty cycle. The experimental data (4,5) is for four different train lengths, two of which are shown in Figures II-9 and II-10. The Army model is limited in train length to 10 seconds, but extrapolation was made for the data at 30-second train lengths. Again, the TOT model is favored by the fit with experiment, and it is recommended for its ease of application while still considering all of the variables.

Efforts were made to justify the empirical fit to the multiple-pulse threshold data by a mechanistic model. It is generally believed that thermal damage is the principal mechanism involved in threshold retinal lesions. It is quite conceivable that subthreshold doses can produce latent damage that becomes visible only after accumulation from repeated doses. Thus, there would be a lowering of threshold energy per pulse for a train of pulses.

The IITRI thermal model for retinal damage (14) incorporates the Henriques damage integral:

$$\Omega = \int e^{C_1} e^{-C_2/T} dt$$

which, in principle, accumulates damage until threshold is reached at $\Omega = 1$. T is the absolute temperature of the tissue which is a function of space and time, and c_1 and c_2 are empirically determined coefficients based on first-order rate processes.

Exercise of the thermal model for multiple pulses produces a threshold profile with very little decrement from the single-pulse value until the rate of heat deposition exceeds the rate of heat dissipation and higher temperatures are reached. This behavior of the thermal model may be understood by considering the Henriques integral. If the temperature-time profile is a square step up and down for time, t, the integral may be readily evaluated:

$$\Omega = t e^{C_1} e^{-C_2/T}.$$

There are two cases where the temperature approaches a step function. One case is long exposures where the temperature rise reaches a steady state and the thermal relaxation time is relatively short. The other case is for very short exposures where the thermal rise time is short compared to relaxation times. In this case, the temperature-time profile approximates an impulse where the amplitude, ΔT, is proportional to the total energy of the pulse. The duration of this impulse, t_i, is of the order of microseconds and is independent of exposure time, t_e. The temperature rise, $\Delta T = T - T_0$, can be calculated for given intervals using the suggested values of the coefficients c_1 and c_2. A temperature rise of $50^\circ C$ produces threshold damage in 10 μsec, while a temperature step of $20^\circ C$ requires ∿10 seconds for the damage integral to reach threshold. Clearly, the reaction time is very sensitive to the amplitude of ΔT.

Assuming that latent damage is irreversible, a train of N thermal pulses would produce a threshold with a damage integral, Ω, of 1/N per pulse. Solving the above equation for ΔT when $\Omega = \frac{1}{N}$ gives:

ADJUSTED TOTAL-ON-TIME (sec) (RTt_b)

TOTAL ENERGY (uJ)
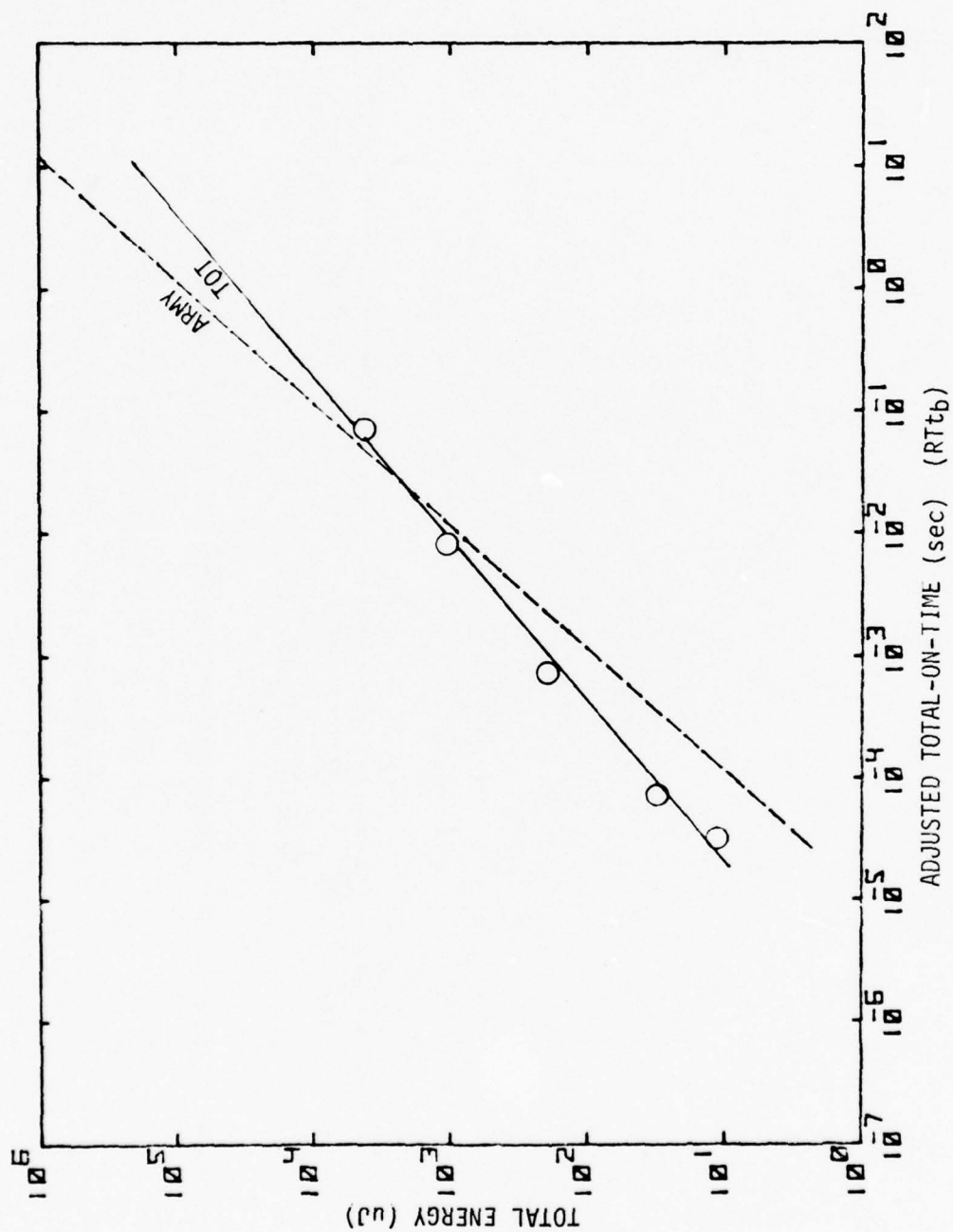
Figure II-9. Comparison of Army and TOT multiple-pulse models.

$T = 0.5$ sec; $\frac{1}{T} < R < \frac{10}{t_bT}$; 1064-nm, 280-nsec pulses.

o - Experimental points from Hemstreet et al. (4)
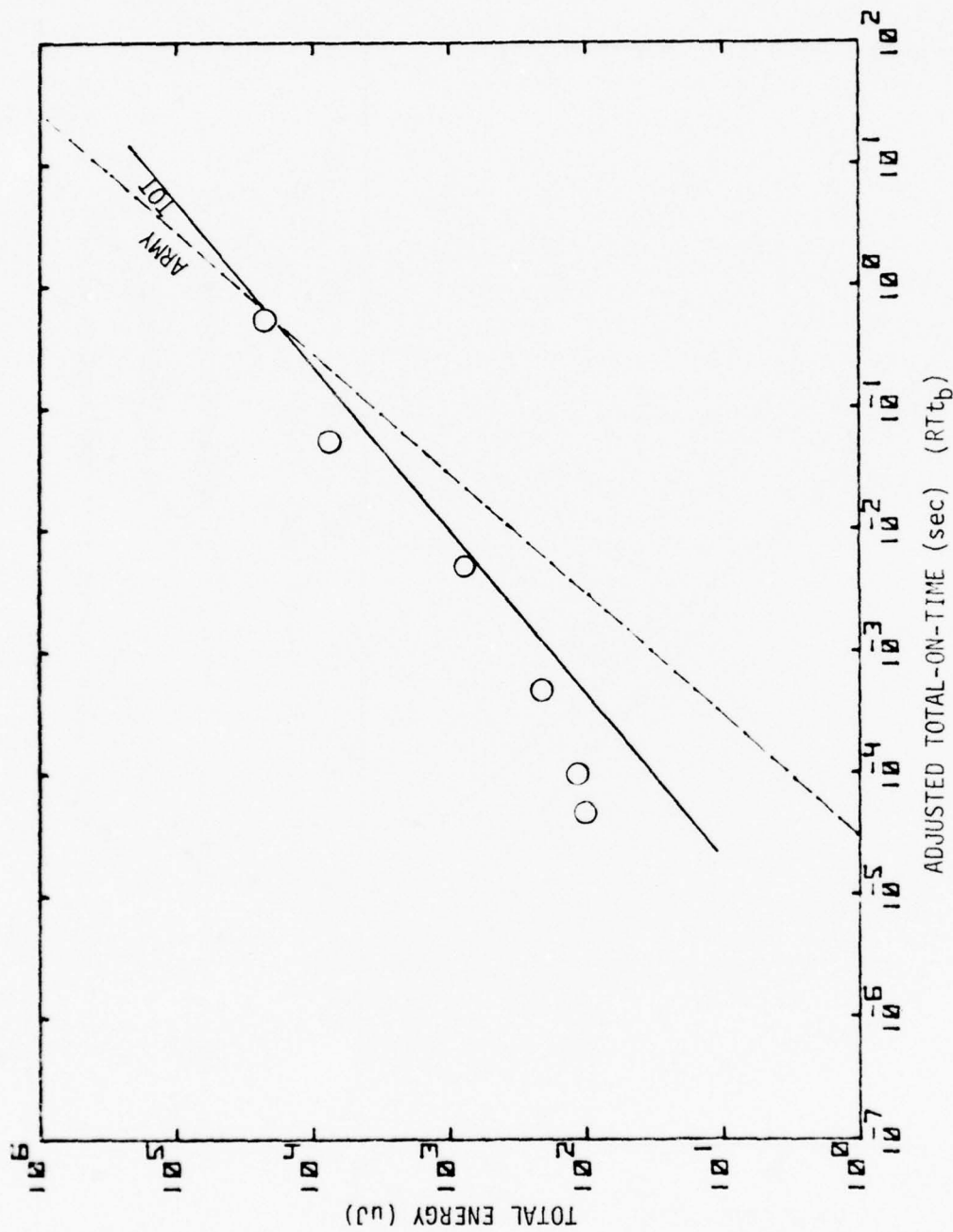
Figure II-10. Comparison of Army and TOT multiple-pulse models.

$T = 30$ sec; $\frac{1}{T} < R < \frac{10}{t_b T}$; 1064-nm, 280-nsec pulses.

o – Experimental points from Hemstreet et al. (4)

$$\Delta T = c_2/(\ln t_i + c_1 + \ln N) - T_0.$$

This indicates that the threshold energy per pulse decreases gradually as the number of pulses increases. The rate of change will depend on the values of c_1, c_2, and t_i. The empirical TOT model gives a decrease of threshold energy per pulse which varies as $N^{-\frac{1}{4}}$. It is difficult to reconcile these two models, and some doubt is raised over both of them. The Henriques integral was originally used to account for damage to porcine skin from long exposures to temperatures between 47° and 53°C (15). It is perhaps hoping too much that the same damage process occurs in an eye exposed to very short pulses. Further work is needed to achieve a clearer picture of the damage mechanism in order that the damage integral may be correctly expressed.

REFERENCES

1. American National Standard for the Safe Use of Lasers. Standard Z136.1. American National Standards Institute, 1976.

2. Skeen, C. H., et al. Ocular effects of repetitive laser pulses. Technology Incorporated, Final Report, Contract F41609-71-C-0018, USAF School of Aerospace Medicine, June 1972.

3. Skeen, C. H., et al. Ocular effects of near infrared laser radiation for safety criteria. Technology Incorporated, Final Report, Contract F41609-71-C-0016, USAF School of Aerospace Medicine, June 1972.

4. Hemstreet, H. W., Jr., J. S. Connolly, and D. E. Egbert. Ocular hazards of picosecond and repetitive-pulsed lasers. Volume I: Nd:YAG laser (1064 nm). SAM-TR-78-20, Apr 1978.

5. Connolly, J. S, H. W. Hemstreet, Jr., and D. E. Egbert. Ocular hazards of picosecond and repetitive-pulsed lasers. Volume II: Argon-ion laser (514.5 nm). SAM-TR-78-21, Apr 1978.

6. Griess, G. A. In Research on the ocular effects of laser radiation. Technology Incorporated, Quarterly Report 3, Part II, Contract F33615-77-C-0615. USAF School of Aerospace Medicine, Dec 1977.

7. Gibbons, W. D. Retinal burn thresholds for exposure to a frequency-doubled neodymium laser. SAM-TR-73-45, Nov 1973.

8. Lund, D. G., D. O. Adams, and C. Carver. Ocular hazard of the gallium-arsenide laser. LAIR-30, 1976.

9. Ebbers, R. W. Retinal effects of multiple-pulse laser. Am Ind Hyg Assoc J 35:252 (1974).

10. Lund, D. J., and E. S. Beatrice. Pulse additivity of neodymium exposures. Letter Report to Project Miles.

11. Ebbers, R. W., and I. L. Dunsky. Retinal damage thresholds for multiple-pulse lasers. Aerospace Med 44:317 (1973).

12. Gibbons, W. D., and D. E. Egbert. Ocular damage thresholds for repetitive pulsed argon laser exposures. SAM-TR-74-1, Feb 1974.

13. Stuck, B. E., D. J. Lund, and E. S. Beatrice. Data base for recommendation of change in Army laser safety regulations. (T. B. Med 279 AR 40-46) in Communication to Members of Z-136 Subcommittee on Bioeffects: Eye, Nov 1977.

14. Takata, A. N., et al. Thermal model of laser-induced eye damage. IIT Research Institute, Final Technical Report, Contract F41609-74-C-0005, USAF School of Aerospace Medicine, Oct 1974.

15. Henriques, F. C., Jr., and A. R. Moritz. Studies of thermal injury. I, II and III. Am J Pathol 23:531, 695 and 915 (1947).

16. Gibson, G. L. M. Retinal damage from repeated subthreshold exposures using a ruby laser photocoagulator. SAM-TR-70-59, Oct 1970.

RESEARCH ON THE OCULAR EFFECTS OF LASER RADIATION

PART III

PATTERN VISUAL EVOKED RESPONSE EVALUATIONS IN ALERT RHESUS MONKEYS

Joseph M. Harrison

INTRODUCTION

The intensity parameters necessary to produce ophthalmoscopically visible corneal and retinal lesions with laser radiation are well documented (1,2). Thermal and photochemical models have been proposed (2,3) to account for the structural damage. The functional disturbances produced by laser radiation with intensities too low to cause ophthalmoscopically visible lesions, though important from the standpoint of safety considerations, have not been thoroughly investigated. Intensities of laser radiation bordering on those producing visible lesions are particularly important. An investigation of the effect of such intensities demands an adequate animal model because of the potential hazard involved. The rhesus monkey is an excellent animal model for this purpose. Anatomically (4) and behaviorally (5), the rhesus visual system has been shown to be identical in most respects to that of humans.

A tool for rapid determination of visual function is necessary to investigate the early time course of functional changes following exposure of the eye to laser radiation, since important effects of high-intensity radiation may be transient (6). In the USAFSAM/RZL laboratory, human visual evoked response (VER) power spectral densities (PSDs) showing easily discriminable components at the contrast-change frequency have been demonstrated with only 5 seconds of recording.

The VER is also capable of detecting peripheral lesions. Fishman and Copenhaver (7) showed that flash stimuli subtending 3 degrees centered on the fovea of an eye with a macular lesion of about 4 degrees produced VERs with amplitudes only one-third of those produced by similar stimulation of the normal eye.

In addition, the VER sensitivity to spatio-temporally patterned stimulation parallels that of psychophysical sensitivity determined under similar conditions. When the contrast of a grating generated on an oscilloscope is set at a psychophysically determined threshold value, the associated VER varies according to whether or not the grating is discriminated (8). The modulation transfer function (MTF; the contrast for a constant response as a function of spatial frequency of a grating) derived from VER data is the same as the psychophysically determined function (9). Blakemore and Campbell (10) showed that the selective spatial frequency adaptation effect is the same whether determined psychophysically or with the VER. The adaptation effect measured both ways depends on orientation of the bars relative to the adaptation stimulus. Psychophysically, the resolving power is better in the horizontal and vertical planes than in the oblique planes. Maffei and Campbell (11) demonstrated,

correspondingly, that the VER is more sensitive to vertical and horizontal gratings than to gratings at other orientations. The amplitude of the VER varies with the frequency disparity of two gratings presented to the two eyes in such a way that the VER is maximal at the disparity producing the greatest sensation of depth (12).

Phase alternating light and dark bar patterns can produce much information about the spatial resolving power or acuity of the visual system when the data are sufficient to derive modulation transfer functions (MTFs). Spatial resolving power is one characteristic of visual function which will change with laser insult to the eye (13). De Valois et al. (5) demonstrated that the MTFs for the rhesus and for man were very similar when determined with the same apparatus under the same conditions. Electrophysiologically determined MTFs for the rhesus can be compared against the behavioral ones already available. Presumably, psychophysical and electrophysiological parallelism will exist for the rhesus as well as for man. However, Padmos et al. (14) showed slight differences between VERs produced by a checkerboard pattern in the anesthetized rhesus and in man. The VER could be explained on the basis of "on-off" ganglion cells and was not the true pattern VER recorded from the scalps of humans.

The VER produced by alternating bar stimuli has not been investigated in the alert rhesus. The normal response to the various parameters of this stimulus must be determined as a baseline against which to compare post-laser exposure VERs. To produce reliable VER data the rhesus must be trained to observe the area where the grating stimuli will be presented. The adequacy of this observation must also be monitored.

The Reaction Time - Observing Response (RTOR) technique resolves both of these problems. This method was described in detail by D. B. Moody (15). The RTOR has already been used with rhesus in pattern-produced VER experiments (16) and in visual cortex unit studies (17, 18). Harwerth and Sperling (19) used this method to control rhesus visual fixation and to determine spectral sensitivity before and after exposure to high-intensity noncoherent radiation.

It is planned to utilize the trained rhesus and the baseline VER data in a project designed to detect visual dysfunctions and to demonstrate the time course of altered visual function following exposure of the rhesus eye to laser radiation. This will be accomplished by using the VER to alternating bar stimuli as a measure of visual function. The laser-induced visual dysfunction studies will be carried out in the Laser Effects Branch, USAFSAM, under work unit 7757-02-53.

<center>METHOD</center>

During the next six months, four male rhesus (<u>Macaca mulatta</u>) monkeys will be trained in the RTOR. A description of the sequence of steps necessary to shape and train the RTOR follows:

1. <u>Leash train</u> - The monkey is habituated to being led around with a collar and leash.

2. <u>Chair train</u> - The monkey is trained to drink from and not manipulate a drink tube using orange juice. The monkey will be trained to sit quietly in the primate chair in the acoustic chamber for an hour.

3. Magazine train - Water deprivation of the monkey is begun. The monkey will be weighed frequently to establish a baseline weight prior to water deprivation. The first days of deprivation will be on weekdays. The monkey will then be allowed to drink water ad libitum from a drink tube gated by a liquid solenoid valve (LSV); the amount of water consumed being measured. Within a few sessions, the monkey should begin to maximize water consumed while in the chair since this will be the only period during the day when water will be available. The average amount of water consumed on the last 2 days of this 5-day adaptation period will be taken as the baseline ad lib water consumption per 24 hr. This will determine the liquid volume to be delivered each session in order to maintain the body weight at 85% of the monkey's projected weight based upon its age according to the rhesus age-weight charts (20). Skin tonicity, general body condition, and body weight will be closely monitored.

After this adaptation period is completed, reinforcement will be delivered only when the monkey is sitting still and facing forward. Reinforcement will be a measured volume of synthetic orange juice (Tang) delivered by operating the LSV. The triggering of the LSV will be accompanied by a pure tone (sonalert) which will be left on for a short period of time as a signal that liquid is available. The criterion for completion of this stage will be a short latency quick sip after the LSV has been triggered.

4. Fixation light train - A Kodak "Carousel 600" slide projector will serve as the fixation light (FL) source. The duration of the FL will be controlled by a Gerbrands R1166 shutter and 300 Series timer-driver. The shutter will be open at the same time and for the same duration as the sonalert (SA) whose duration is now fixed. The FL will appear on a transilluminated diffusing screen in the center of the observing area. The experimenter will reinforce the monkey for sitting still and looking toward the observing area. This step will habituate the monkey to the FL.

5. Lever train - After the monkey is trained to sit quietly and face the observing area for 30 sec, a lever connected to a microswitch will be introduced.

   a. The monkey will be reinforced for sitting still, looking toward the observing area, and pressing the lever.

   b. The monkey will be rewarded only once for multiple presses occuring during the fixed duration of SA and FL.

6. Limited hold train - After the monkey is trained to press the lever to get the liquid, the SA and FL, it will be trained to press the lever and not to release it until a certain amount of time has elapsed.

   a. FL, whose duration is now very short (100 msec), is automatically triggered by a lever press and the SA and LSV by a lever release. Lever release is automatically rewarded if it occurs during a reward period (RP) beginning 100 msec after the lever press and ending 2 sec after the lever press. (As the duration of the FL is increased, the beginning of the RP is correspondingly delayed. RP always begins at the end of FL.)

b. FL duration is lengthened. When the monkey begins to make a time discrimination (i.e., press lever and hold for a time period and release to get reward, thus not paying attention to FL), the duration of FL will be varied randomly.

c. Duration of RP is shortened from the far end (i.e., from the end furthest from the termination of the FL). The final RP duration will be 0.7 sec.

d. The contrast of FL is gradually reduced.

e. The size of FL is gradually reduced to approach a 30-sec low contrast spot.

f. The observing area is now a TV screen with alternating bars. A circular portion of the TV screen is seen surrounded by the diffusing screen. A beam splitter is introduced to project the FL image to the center of, and at the plane of, the observing area (TV screen).

g. Scalp electrodes (attached with colloidin) and ear electrodes are gradually introduced. Figure III-1 depicts a flow diagram for the final trained RTOR.

The training procedure will be automated by a Digi-Bit program. A block diagram of this apparatus appears in Figure III-2. When the RTOR has been completely trained and the monkey is habituated to the presence of the scalp and ear electrodes, determination of the baseline VER to the alternating bars generated on the TV screen can begin. The stimuli presented in the observation area will consist of a FL inside a circular area of the TV screen subtending six degrees at the retina. This observing area will be surrounded by a rectangular transilluminated diffusing screen with a brightness approximately equal to the average brightness of the TV screen and subtending 15 x 20 degrees at the retina. The alternating bar pattern will be presented in the observing area periodically while the rhesus is observing the FL. This grating is produced on the TV screen by a Counterphase Grating Stimulator developed by Technology Incorporated. Synchronization with the signal averager is also produced by this instrument. Figure III-3 diagrams the Stimulus Presentation System. Signals will be led from the scalp in a monopolar single ended configuration to a Grass 7P511 amplifier with an amplification of 100,000. The output of the amplifiers will go to a Tektronix 5512 oscilloscope and a Grass 78D EEG/Polygraph for monitoring, and also to an Ampex PR2200 tape recorder. The signals can be led on-line or from magnetic tape off-line to the Nuclear Data 100 Multichannel Analyzer for producing averaged VERs or to the Digital Equipment Corporation PDP 11-34 for producing averaged VERs, Fast Fourier Transforms (FFT), and power spectral densitites (PSD) with printouts on a Versatec D1200A printer/plotter. The FFT can be done on either the averaged (i.e., VER) or the unaveraged EEG.

The dependent variables to be analyzed are the form, amplitude, and implicit times of the averaged VERs and the amplitudes of the frequency components of the PSDs. Transformations of the dependent variables will include MTFs determined either from the averaged VERs or the PSDs. For each spatial frequency of the grating, the contrast will be varied to produce contrast by amplitude or implicit time functions. There is a linear relation between log contrast and amplitude of the VER (8). The contrast either at some constant
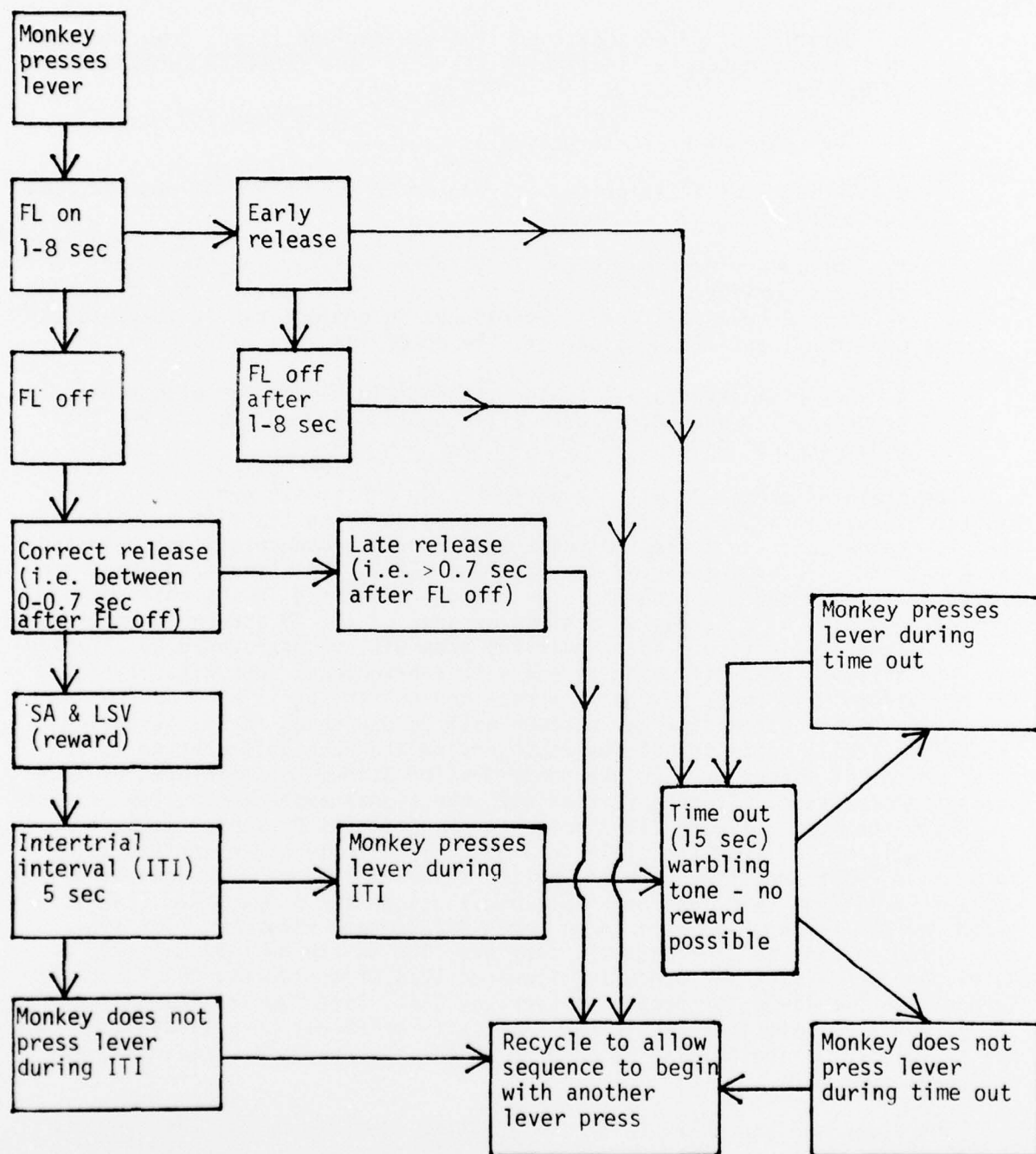
Figure III-1. Flow diagram for the final trained RTOR.
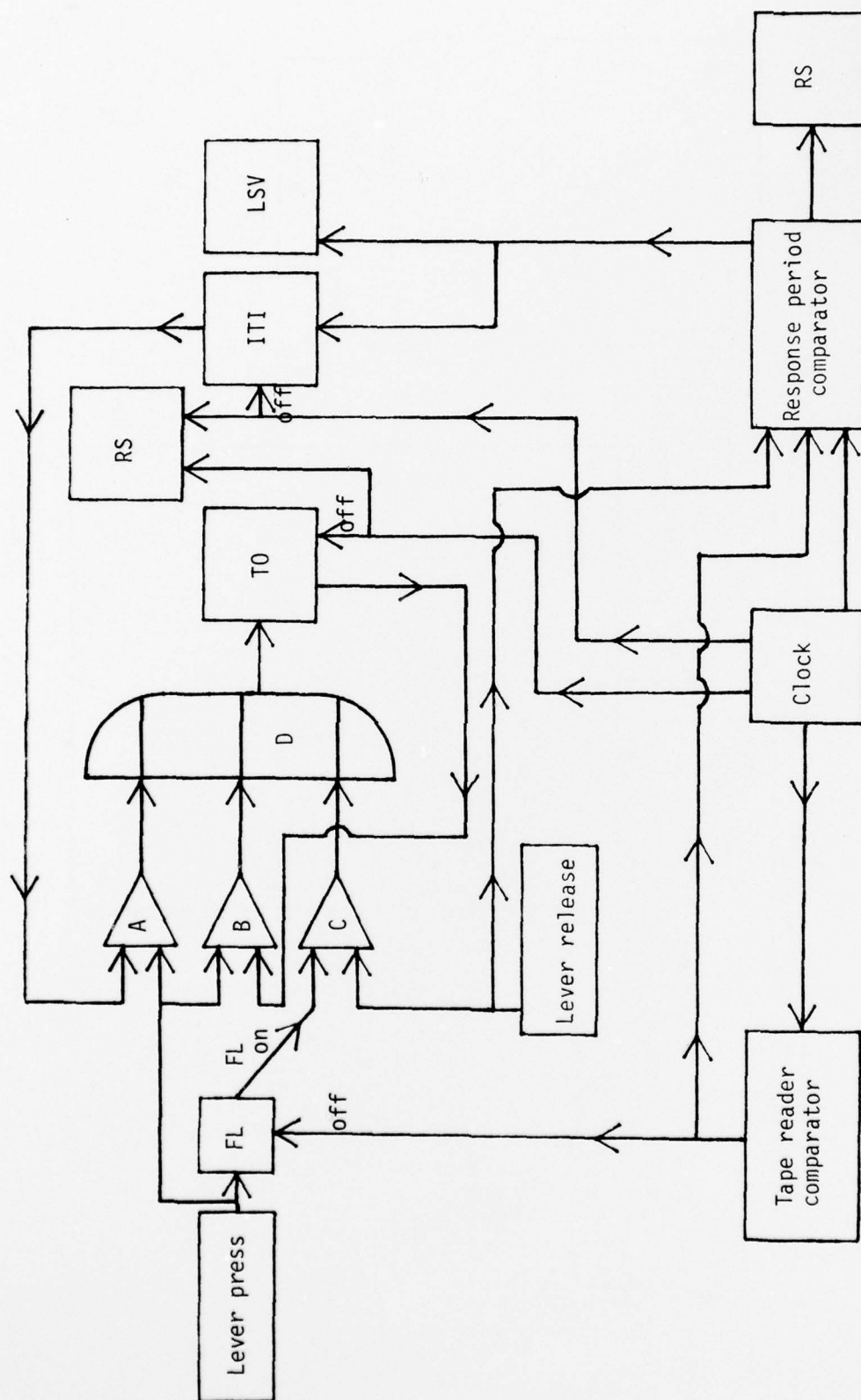
Figure III-2. Schematic of the automated training apparatus. A, B, and C are symbols for "and" logic; D, symbol for "or" logic; FL, fixation light; ITI, intertrial interval; LSV, liquid solenoid valve; RS, reset pulse; TO, time out.

A Large diffusing screen
B Plate glass windows
C Beam splitter
D Filter & lens holder
E Small diffusing screen
F Lens
G Shutter
H Projector
I Television
J Shutter driver
M Monkey

Figure III-3. Diagram of the stimulus presentation system.

voltage criterion (above 0 volts) obtainable for all spatial frequencies or at the extrapolated zero voltage VER will be one point in the spatial frequency MTF.

Initial efforts will be aimed at establishing a baseline VER against which post-laser-exposure VER data can be compared. When this has been completed, electrodes will be implanted on the dura overlying the foveal projection area of the monkey visual cortex. Electrodes will also be implanted in the ipsilateral abducens and contralateral oculomotor nucleus and a pedestal attached following the method of Wolfe (21) for control of eye position and head restraint. Before lase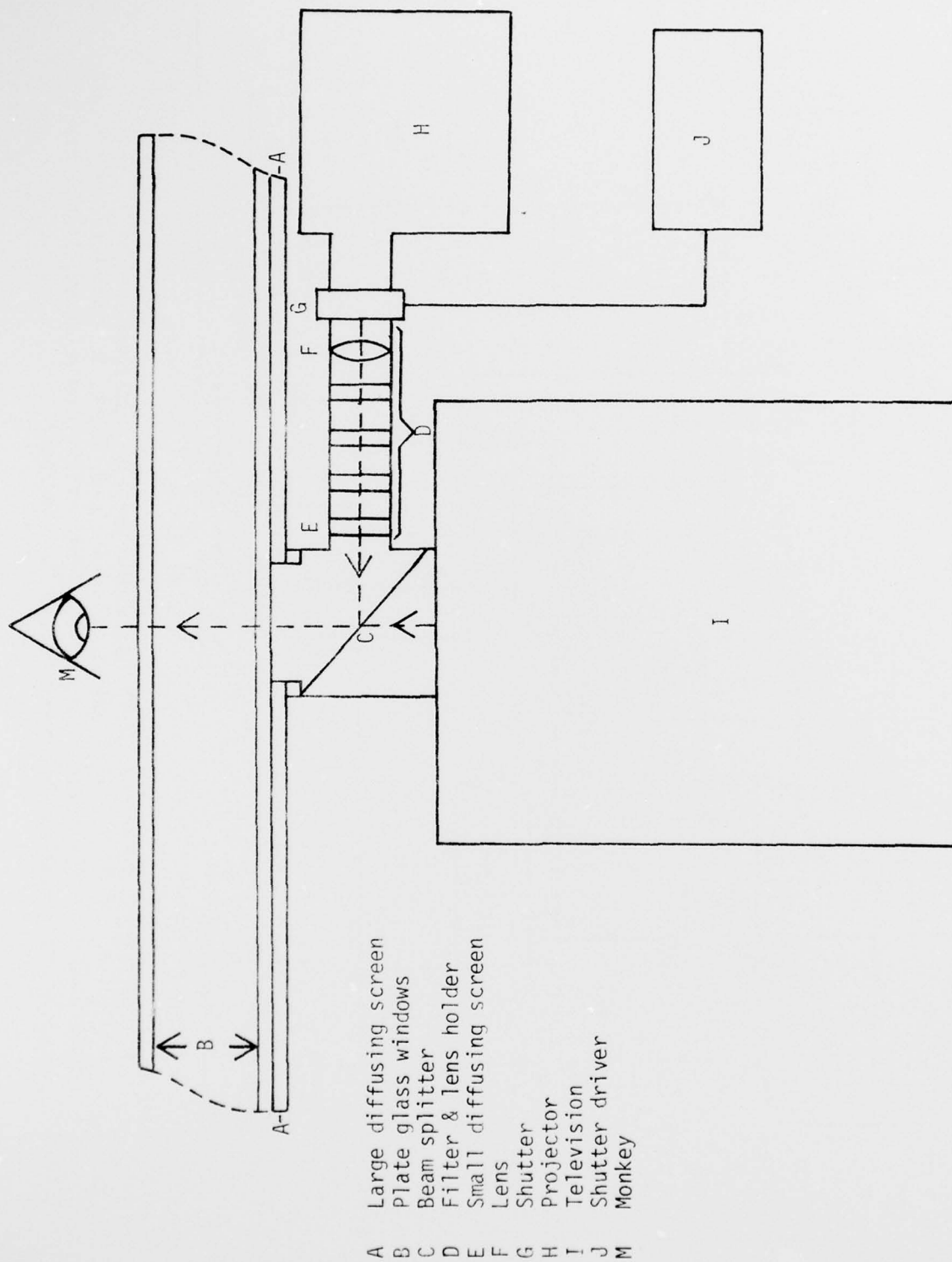r exposure, the monkey will be allowed to recuperate and reach stable response in the RTOR. A spot check of the VERs will be done since the signals from the dural electrodes will almost certainly be slightly different from those recorded from the scalp. When enough data has been collected to establish this new baseline response, the monkeys can be exposed to laser radiation. The exposure conditions will include variations in both exposure time and wavelength. The initial laser exposures will be at levels below those known to produce retinal damage. Subsequently, exposures will be increased stepwise to levels which will produce visible damage. The laser-induced visual dysfunction studies will be part of work unit 7757-02-53, and the laser exposures and subsequent VER recordings will follow the protocols established for that work unit.

Post-exposure VERs will be elicited in the same way as the pre-laser-exposure VERs. The dependent variables and the transformations of these variables will be compared to those preceding laser exposures.

RESULTS

At this time, two male rhesus monkeys have been examined and found to have no retinal abnormalities observable with the Zeiss fundus camera and to have dioptric errors of less than 0.5 diopters as measured with a slit lamp retinoscope. The canines have been removed and collars and leashes attached. Both monkeys have completed chair training.

The author is participating in a study being conducted in the Laser Effects Branch of the USAF School of Aerospace Medicine to determine VER baseline data recorded from anesthetized paralyzed monkeys. Data from this study will be used to guide the placement of scalp electrodes and as an indication of the optimal range of alternating bar parameters for production of maximal VERs recorded from the unanesthetized behaving monkey.

REFERENCES

1. Vassiliadis, A. Ocular damage from laser radiation. In M. L. Wolbarsht (ed.). Laser applications in medicine and biology, Ch 6. New York: Plenum Press, 1971.

2. Wolbarsht, M. L., and D. H. Sliney. The formulation of protection standards for lasers. In M. L. Wolbarsht (ed.). Laser applications in medicine and biology, Ch 10. New York: Plenum Press, 1971.

3. Barnes, I. S. Biological damage resulting from thermal pulses. In M. L. Wolbarsht (ed.). Laser applications in medicine and biology, Vol. II, Ch 6. New York: Plenum Press, 1974.

4. Polyak, S. L. The vertebrate visual system. Chicago: University of Chicago Press, 1957.

5. De Valois, R. L., H. C. Morgan, and M. Snodderly. Psychophysical studies of monkey vision. III. Spatial luminance contrast sensitivity tests of macaque and human observers. Vis Res 14:75 (1974).

6. Auerbach, E., and G. Wald. The participation of different types of cones in human light and dark adaptation. Am J Ophthalmol 39:24 (1955).

7. Fishman, R. S., and R. M. Copenhaver. Macular disease and amblyopia: the visual evoked response. Arch Ophthalmol 77:718 (1967).

8. Campbell, F. W., and J. J. Kulikowski. An electrophysiological measure of the psychophysical contrast threshold. *J Physiol (London)* 217:54P (1971).

9. Campbell, F. W., and L. Maffei. Electrophysiological evidence for the existence of orientation and size detectors in the human visual system. J Physiol (London) 207:635 (1970).

10. Blakemore, C., and F. W. Campbell. On the existence of neurones in the human visual system selectively sensitive to the orientation and size of retinal images. J Physiol (London) 203:237 (1969).

11. Maffei, L., and F. W. Campbell. Neurophysiological localization of the vertical and horizontal visual coordinates in man. Science 167:386 (1970).

12. Fiorentini, A., and L. Maffei. Electrophysiological evidence for binocular disparity detectors in human visual system. Science 169:208 (1970).

13. Robbins, D. O., H. Zwick, and G. C. Holst. A method for producing foveal retinal exposures in an awake, task oriented, rhesus monkey. Behav Res Meth Instru 5:457 (1973).

14. Padmos, P., J. J. Haaijman, and H. Spekreijse. Visually evoked cortical potentials to patterned stimuli in monkey and man. EEG Clin Neurophysiol 35:153 (1973).

15.   Moody, D. B.   Reaction time as an index of sensory function.   In W. C.
      Stebbins (ed.).   Animal psychophysics: The design and conduct of sensory
      experiments, Ch 10.   New York: Appleton-Century-Crofts, 1970.

16.   Doddington, H.   Activity evoked in the visual system of human, rhesus mon-
      key, and cat by spatially patterned and non-patterned visual stimuli.
      Unpublished Dissertation, University of Florida, 1972.

17.   Wurtz, R. H.   Visual receptive fields of striate cortex neurons in awake
      monkeys.   J Neurophysiol 32:727 (1969).

18.   Poggio, G. F., R. W. Doty, Jr., and W. H. Talbot.   Foveal striate cortex
      of behaving monkey: Single-neuron responses to square wave gratings
      during fixation of gaze. J Neurophysiol 40:1369 (1977).

19.   Harwerth, R. S., and H. G. Sperling.   Prolonged color blindness induced
      by intense spectral lights in rhesus monkeys.   Science 174:520 (1971).

20.   Van Wagenen, G., and H. R. Catchpole.   Physical growth of the rhesus mon-
      key (Macaca mulatta).   Am J Phys Anthropol 14:245 (1956).

21.   Wolfe, J. W.   Technique for chronic head restraint and electrophysiological
      recording in the awake rhesus monkey.   Physiol Behav 13:461 (1964).

RESEARCH ON THE OCULAR EFFECTS OF LASER RADIATION

PART IV

ELECTRONICS AND SOFTWARE FOR THE VISUAL STIMULUS LAB

James C. Brakefield

The effort to build and test an electronic controller which will interface to the PDP 11/34 computer began in February 1978.

A master schematic was prepared. This showed most of the circuitry in abbreviated form. Accompanying literature was prepared to describe the characteristics and operation of the controller. Sessions were held between Technology Incorporated and the Laser Effects Branch, USAFSAM, to determine the exact characteristics of the controller.

The master schematic was used to partition the circuitry into five circuit boards and a backplane. Schematics were prepared for each board and the backplane and represent the working documents.

The five circuit boards are:

1. X and Y ramp generators
2. Master oscillator and control board
3. X memory board
4. Y memory board
5. "Z" axis or intensity board

Parts were selected and ordered. The major part categories are:

1. Wire wrap sockets, circuit boards, backplane
2. Power supplies
3. Digital-to-analog converters
4. High-speed memory
5. Low-power Schottky parts from the TTL logic series

A block diagram of the controller is shown in Figure IV-1. Computer access to the device is through a parallel I/O port. Connection to the visual stimulator is via coaxial cabling.

Construction of the circuit boards has begun. A hardware schedule is shown below. It also functions as a checklist. Typically, work is in progress on several items simultaneously.

Hardware Schedule - Electronic Controller

Design
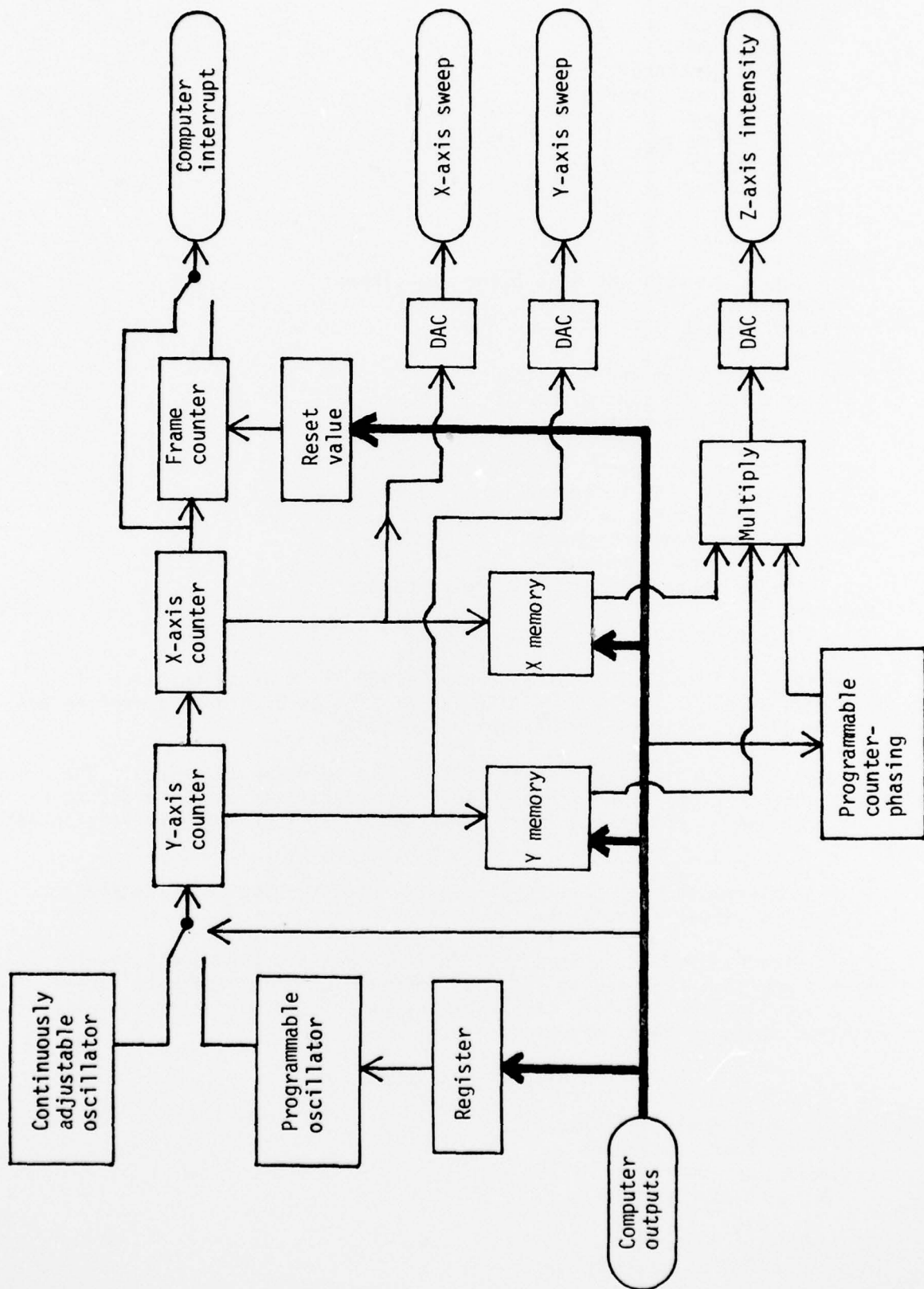   Master Schematic
    Operator interface

70

Figure IV-1. Visual stimulator electronic controller.

71

Computer interface
            Board allocation
            Detail schematics
                  Ramp generator
                  Clock and control
                  X memory
                  Y memory
                  Intensity
                  Backplane
            Parts list
            Wiring list
      Breadboard
            Mount IC sockets and decoupling capacitors
            Wire wrap
            Check wiring
            Mount IC's
      Offsite test, debug and operate
            Test clock and control board
            Test ramp generator
            Test memory boards
            Test intensity board
            Test boards with backplane
            Simulate computer hookup and test
      Onsite test, debug and operate
            Write diagnostic software
            Test and debug hardware using diagnostics
      Document
      Maintain and update

     An effort to improve the software on the PDP 11/34 began in March 1978.
Consultations were held with the USAFSAM Laser Effects Branch personnel to de-
termine the characteristics of the desired software.

     A human interface is required as well as the hardware interface. The human
interface characteristics went through several simplifications in order to re-
duce the programming effort required. The coding for a preliminary version was
begun.

     It is anticipated that this same software will be used to drive the con-
troller for the visual stimulator.

     The software schedule is less well defined than the hardware schedule.
The reasons are that the task is less well defined and that software manage-
ment itself is less well understood. The following schedule attempts to show
the required steps in this software project.

                              Software Schedule

      Determine hardware interface
      Define software interface
      Define human interface
            Consult with end users
            Specify
            Iterate
      Design software organization

Must meet requirements of:
                  Maintainability
                  Flexibility
                  Cost
                  Capability (i.e., performance)
             Must have a conceptional unity
        Code and debug
             Should be done in a top-down fashion, i.e., do the human interface
             first
        Document
             Actually, this should be done at the same time as coding
        Iterate until satisfied
        Maintain and update

     Figure IV-2 shows the original progress chart for the electronic control-
ler project. This report covers months 1 and 2.

TASK DESCRIPTION	1	2	3	4	5	6	7	8	9	10	11	12
Design	↕	↕										
Breadboard & Construct		↕			↕							
Test, Debug and Operate					↕		↕					
Software Development	↕										↕	
Design Study, Parts List, Cost Estimate & Schematic for Color System			↕									↕

MONTHS

Figure IV-2. Project planning document for stimulator for visual evoked responses.

74